NASA TECHNICAL MEMORANDUM

NASA TM X-74018

NASA TM X-74018

LOW-SPEED WIND-TUNNEL RESULTS FOR A MODIFIED 13-PERCENT-THICK AIRFOIL

Robert J. McGhee and William D. Beasley

National Aeronautics and Space Administration

Langley Research Center
Hampton, Virginia 23665

Low-Speed Wind-Tunnel Results for a Modified 13-Percent-Thick Airfoil

Robert J. McGhee and William D. Beasley
Langley Research Center

SUMMARY

An investigation was conducted in the Langley low-turbulence pressure tunnel to evaluate the effects on performance of modifying a 13-percent-thick low-speed airfoil. The airfoil contour was altered to reduce the aft upper-surface pressure gradient and hence delay boundary-layer separation at typical climb lift coefficients for light general aviation airplanes. The tests were conducted at a Mach number of 0.15 or less over a Reynolds number range from about 1.0×10^6 to 9.0×10^6. The geometric angle of attack varied from about -10° to 20°.

The results indicate that the modification to the airfoil contour increased the maximum lift-drag ratio about 12 percent at a Reynolds number of 2.0×10^6 but that essentially no improvement was obtained at Reynolds numbers of 4.0×10^6 and 6.0×10^6. The results also indicate that the modification to the airfoil decreased the maximum lift coefficient about 0.04 throughout the Reynolds number range tested. The theoretical viscous analysis method employed proved to be a valuable tool in predicting the airfoil pressure distributions and boundary-layer separation points.

INTRODUCTION

Research on an initial thickness family of airfoils developed for low-speed general aviation application is reported in reference 1. Results of

this research showed that the 13-percent-thick airfoil provided the best performance for this initial thickness family of airfoils. This airfoil, which is designated as the NASA LS(1)-0413 airfoil, has been modified in an attempt to further improve the low-speed performance. The airfoil contour was changed to reduce the aft upper-surface pressure gradient and hence delay boundary-layer separation at typical climb lift coefficients for light general aviation airplanes. This report presents the basic low-speed section characteristics of this modified airfoil and evaluates the effects on performance resulting from the change in airfoil shape.

The investigation was performed in the Langley low-turbulence pressure tunnel at Mach numbers of 0.15 or less. The chord Reynolds number varied from about 1.0×10^6 to 9.0×10^6 and the geometrical angle of attack varied from about -10° to 20°.

SYMBOLS

Values are given in both SI and U.S. Customary Units. The measurements and calculations were made in the U.S. Customary Units.

c_p pressure coefficient, $\frac{p_L - p_\infty}{q_\infty}$

c airfoil chord, centimeters (inches)

c_c section chord-force coefficient, $\oint c_p \, d\left(\frac{z}{c}\right)$

c_d section profile-drag coefficient, $\int_{\text{wake}} c'_d \, d\left(\frac{h}{c}\right)$

c'_d point drag coefficient (ref. 5)

c_l section lift coefficient, $c_n \cos \alpha - c_c \sin \alpha$

c_m section pitching-moment coefficient about quarter-chord point, $-\oint C_p \left(\frac{x}{c} - 0.25\right) d\left(\frac{x}{c}\right) + \oint C_p \left(\frac{z}{c}\right) d\left(\frac{z}{c}\right)$

c_n section normal-force coefficient, $-\oint C_p \, d\left(\frac{x}{c}\right)$

h vertical distance in wake profile, centimeters (inches)

M free-stream Mach number

p static pressure, N/m^2 (lb/ft^2)

q dynamic pressure, N/m^2 (lb/ft^2)

R Reynolds number based on free-stream conditions and airfoil chord

S separation point

t airfoil thickness, centimeters (inches)

x airfoil abscissa, centimeters (inches)

z airfoil ordinate, centimeters (inches)

z_c mean line ordinate, centimeters (inches)

z_t mean thickness, centimeters (inches)

α geometric angle of attack, degrees

Subscripts:

L local point on airfoil

max maximum

∞ undisturbed stream

Abbreviations:

LS(1) low-speed first series

Mod modified

AIRFOIL MODIFICATION

The airfoil contour was changed to reduce the aft upper-surface pressure gradient (fig. 1) and hence reduce boundary-layer separation at typical climb lift coefficients for light general aviation airplanes (c_l = 1.0 to 1.2). The maximum thickness ratio, trailing-edge thickness, and design lift coefficient (c_l = 0.40) of the original airfoil were retained.

The modification to the surface contour of airfoil LS(1)-0413 is illustrated in figure 1. The upper surface modification was accomplished by adding material from approximately the 2.5 percent chord station fairing with the original airfoil at the 40 percent chord station and removing material from this station to the airfoil trailing edge. The lower surface modification was accomplished by adding material from approximately the 50 percent chord station to the airfoil trailing edge. The maximum thickness of the modified airfoil was moved forward about 5 percent chord. Figure 2 compares the change in mean thickness and camber distributions for the two airfoils and figure 3 compares the changes in surface slope distributions. Coordinates for both airfoils are given in tables I and II.

The theoretical viscous analysis computer program of reference 2 was used to predict the pressure distributions and boundary-layer separation points for the airfoils. Boundary-layer transition was specified at x/c = 0.03 for the theoretical calculations to ensure a turbulent boundary-layer development on the airfoils. Figure 4 shows the theoretical results for both airfoils at Reynolds numbers of 2.0×10^6 and 4.0×10^6. At a lift coefficient of 0.40 and a Reynolds number of 2.0×10^6 (fig. 4(a)) both airfoils are separation free. At a lift coefficient of 1.20 the theory indicates a decrease in upper-

surface separation of about 0.05c for the modified airfoil (reduced pressure gradient). At this same lift coefficient (c_l = 1.20) and a Reynolds number of 4.0 x 10^6 (fig. 4(b)) a decrease in separation of only about 0.02c is shown for the modified airfoil. Based on these theoretical results, improvements in performance for the modified airfoil at climb lift coefficients would be expected, particularly at a Reynolds number of 2.0 x 10^6. Since the theoretical method is only valid for attached or boundary-layers with small amounts of flow separation, the maximum lift coefficients for the airfoils could not be determined from the theory.

MODELS, APPARATUS, AND PROCEDURE

Models

The airfoil models were constructed utilizing a metal core around which plastic fill and two thin layers of fiberglass were used to form the contour of the airfoils. The models had chords of 61 cm (24 in.) and spans of 91.44 cm (36 in.). The models were equipped with both upper and lower surface orifices located 5.08 cm (2 in.) off the midspan. The airfoil surface was sanded in the chordwise direction with number 400 dry silicon carbide paper to provide a smooth aerodynamic finish. The model contour accuracy was generally within $\pm$.10 mm (.004 in.).

Wind Tunnel

The Langley low-turbulence pressure tunnel (ref. 3) is a closed-throat, single-return tunnel which can be operated at stagnation pressures from 1 to 10 atmospheres with tunnel-empty test section Mach numbers up to 0.42 and 0.22, respectively. The maximum unit Reynolds number is about 49 x 10^6 per meter

(15 x 10^6 per foot) at a Mach number of about 0.22. The tunnel test section is 91.44 cm (3 ft) wide by 228.6 cm (7.5 ft) high.

Hydraulically actuated circular plates provided positioning and attachment for the two-dimensional model. The plates are 101.60 cm (40 in.) in diameter, rotate with the airfoil, and are flush with the tunnel wall. The airfoil ends were attached to rectangular model attachment plates (fig. 5) and the airfoil was mounted so that the center of rotation of the circular plates was at 0.25c on the model reference line. The air gaps at the tunnel walls between the rectangular plates and the circular plates were sealed with flexible sliding metal seals, shown in figure 5.

Wake Survey Rake

A fixed wake survey rake (fig. 6) at the model midspan was cantilever mounted from the tunnel sidewall and located one chord length behind the trailing edge of the airfoil. The wake rake utilized total-pressure tubes, 0.1524 cm (0.060 in.) in diameter, and static-pressure tubes, 0.3175 cm (0.125 in.) in diameter. The total-pressure tubes were flattened to 0.1016 cm (0.040 in.) for 0.6096 cm (0.24 in.) from the tip of the tube. The static-pressure tubes each had four flush orifices drilled 90° apart and located 8 tube diameters from the tip of the tube and in the measurement plane of the total-pressure tubes.

Instrumentation

Measurements of the static pressures on the airfoil surfaces and the wake rake pressures were made by an automatic pressure-scanning system utilizing variable-capacitance-type precision transducers. Basic tunnel pressures were measured with precision quartz manometers. Angle of attack was measured with

a calibrated digital shaft encoder operated by a pinion gear and rack attached to the circular model attachment plates. Data were obtained by a high-speed acquisition system and recorded on magnetic tape.

TESTS AND METHODS

The modified airfoil was tested at Mach numbers of 0.15 or less over an angle-of-attack range from about -10° to 20°. Reynolds number based on the airfoil chord was varied from about 1.0×10^6 to 9.0×10^6. The airfoil was tested both smooth (natural transition) and with roughness located on both upper and lower surfaces at 0.075c. The roughness was sized for each Reynolds number according to reference 4. The roughness consisted of granular-type strips 0.127 cm (0.05 in.) wide, sparcely distributed, and attached to the airfoil surface with clear lacquer.

The static-pressure measurements at the airfoil surface were reduced to standard pressure coefficients and machine integrated to obtain-section normal-force and chord-force coefficients and section pitching-moment coefficients about the quarter chord. Section profile-drag coefficient was computed from the wake-rake total and static pressures by the method reported in reference 5.

An estimate of the standard low-speed wind-tunnel boundary corrections (ref. 6) amounted to a maximum of about 2 percent of the measured coefficients and these corrections have not been applied to the data.

PRESENTATION OF RESULTS

The results of this investigation have been reduced to coefficient form and are presented in the following figures:

DISCUSSION

The airfoil contour modification produced the theoretically predicted decrease in aft upper-surface pressure gradient shown by the experimental pressure data comparison for both airfoils in figure 10. Note (fig. 10(a)) that altering the shape of the LS(1)-0413 airfoil to reduce the aft upper-surface pressure gradient and retain the design lift coefficient of 0.40 removed the characteristic flat-type pressure distribution. Thus, the modified airfoil exhibits a gradual pressure recovery of nearly uniform slope over approximately 50 percent of the upper surface. Figure 10(b) shows the decrease in upper-surface boundary-layer separation at $\alpha = 10^{0}$ and $R = 2.0 \times 10^{6}$ for the modified airfoil as predicted by the viscous analysis method of reference 2 and discussed under "Airfoil Modification." Boundary-layer separation is indicated by the lack of pressure gradient on the upper surface near the trailing edge of the airfoils. At $\alpha = 10^{0}$ and $R = 4.0 \times 10^{6}$,

(fig. 10(c)) the pressure distributions for both airfoils indicate less but about equal amounts of upper-surface trailing-edge separation. This trend of decreased separation at higher Reynolds numbers was also indicated by the theoretical method. Figure 10(d) compares the pressure data for the two airfoils at $\alpha \approx 16^0$ and $R \approx 2.0 \times 10^6$. For this angle of attack airfoil LS(1)-0413 has reached $c_{l_{max}}$ and upper surface separation extends from about x/c = 0.65 to the trailing edge. The LS(1)-0413 Mod airfoil is fully stalled at this angle of attack and separation extends from about x/c = 0.25 to the trailing edge. This difference in behavior near stall is attributed to the absence of the reduced pressure-gradient near the airfoil mid-chord for the modified airfoil. (See fig. 10(b)). This reduced pressure-gradient retards the rapid forward movement of upper-surface separation at high angles of attack.

The section characteristics for both airfoils are compared in figure 8 for Reynolds numbers of 2.0×10^6, 4.0×10^6, and 6.0×10^6. For a Reynolds number of 2.0×10^6 (fig. 8(a)) and angles of attack from about 4^0 to 13^0 the modified airfoil generates more lift and less drag compared to the original airfoil. This result is attributed to less upper-surface separation for the modified airfoil with the reduced pressure gradient. Thus, the lift-curve is more linear at high angles of attack compared to the lift-curve for the original shape. An improvement in maximum lift-drag ratio of about 12 percent is indicated for the modified airfoil. However, the angle of attack for maximum lift was reduced about 3^0 and hence $c_{l_{max}}$ decreased about 0.04 for the modified airfoil. The stall characteristics for both airfoils were similar. At the higher Reynolds numbers (figs. 8(b) and 8(c)) the capability for improvement in performance over that obtained at $R = 2.0 \times 10^6$

for the modified airfoil was not available and therefore none occurred. However, the same earlier airfoil stall and decrease in $c_{l_{max}}$ were exhibited by the modified airfoil as was previously noted at the lower Reynolds number. The absence of the improvement in performance for the modified airfoil at the higher Reynolds numbers is not surprising, since the turbulent boundary-layer thickness is decreased at the higher Reynolds numbers and therefore can withstand increased pressure gradients before separating. Figure 11 compares the values of $c_{l_{max}}$ for both airfoils for a Reynolds number range from about 2.0×10^6 to 9.0×10^6. The modified airfoil exhibits a loss in $c_{l_{max}}$ of about 0.04 throughout the Reynolds number range. The less negative values of pitching-moment coefficients for the LS(1)-0413 Mod airfoil compared to the LS(1)-0413 airfoil (fig. 8) are associated with the reduction in aft camber which resulted from altering the upper-surface pressure gradient for the modified airfoil and which is illustrated by the comparison of camber distributions of figure 2.

CONCLUDING REMARKS

Low-speed wind-tunnel tests have been conducted in the Langley low-turbulence pressure tunnel to evaluate the effects on performance of modifying a 13-percent-thick airfoil. The airfoil contour was altered to reduce the aft upper-surface pressure gradient and hence delay boundary-layer separation at typical climb lift coefficients for light general aviation airplanes. The tests were conducted over a Reynolds number range from about 1.0×10^6 to 9.0×10^6.

The results show that the modification to the airfoil contour increased the maximum lift-drag ratio about 12 percent at a Reynolds number of 2.0×10^6

but that essentially no improvement was obtained at Reynolds numbers of 4.0×10^6 and 6.0×10^6. Also, the results show that the modification to the airfoil decreased the maximum lift coefficient about 0.04 throughout the Reynolds number range tested. The theoretical viscous analysis method employed proved to be a valuable tool in predicting the airfoil pressure distributions and boundary-layer separation points.

REFERENCES

1. McGhee, Robert J.; and Beasley, William D.: Effects of Thickness on the Aerodynamic Characteristics of an Initial Low-Speed Family of Airfoils for General Aviation Applications. NASA TM X-72843, 1976.
2. Bauer, F.; Garabedian, P.; Korn, D.; and Jameson, A.: Supercritical Wing Section II. Lecture Notes in Economics and Mathematical Systems, M. Beckmann and H. P. Lunzi, eds., Springer-Verlag, c. 1975.
3. Von Doenhoff, Albert E.; and Abbott, Frank T., Jr.: The Langley Two-Dimensional Low-Turbulence Pressure Tunnel. NACA TN 1283, 1947.
4. Braslow, Albert L.; and Knox, Eugene C.: Simplified Method for Determination of Critical Height of Distributed Roughness Particles for Boundary-Layer Transition at Mach Numbers From 0 to 5. NACA TN 4363, 1958.
5. Pankhurst, R. C.; and Holder, D. W.: Wind Tunnel Technique. Sir Isaac Pitman and Sons, Ltd., London, 1965.
6. Pope, Alan; and Harper, John J.: Low-Speed Wind-Tunnel Testing. John Wiley and Sons, Inc., New York, 1966.

TABLE I.- LS(1)-0413 AIRFOIL COORDINATES

x/c	z/c, upper	z/c, lower
0.00000	0.00000	0.00000
.00200	.01040	-.00500
.00500	.01590	-.00940
.01250	.02420	-.01450
.02500	.03320	-.01910
.03750	.03970	-.02230
.05000	.04480	-.02500
.07500	.05260	-.02940
.10000	.05860	-.03280
.12500	.06350	-.03560
.15000	.06750	-.03790
.17500	.07100	-.03980
.20000	.07400	-.04140
.22500	.07650	-.04270
.25000	.07860	-.04370
.27500	.08030	-.04430
.30000	.08180	-.04480
.32500	.08300	-.04510
.35000	.08380	-.04520
.37500	.08430	-.04500
.40000	.08460	-.04470
.42500	.08460	-.04420
.45000	.08440	-.04350
.47500	.08380	-.04260
.50000	.08290	-.04140
.52500	.08170	-.03990
.55000	.08020	-.03810
.57500	.07830	-.03590
.60000	.07610	-.03330
.62500	.07330	-.03050
.65000	.07020	-.02740
.67500	.06670	-.02420
.70000	.06290	-.02100
.72500	.05870	-.01770
.75000	.05420	-.01440
.77500	.04950	-.01130
.80000	.04450	-.00830
.82500	.03930	-.00570
.85000	.03400	-.00350
.87500	.02840	-.00180
.90000	.02270	-.00080
.92500	.01690	-.00060
.95000	.01100	-.00130
.97500	.00480	-.00340
1.00000	-.00160	-.00710

TABLE II.- LS(1)-0413 MOD AIRFOIL COORDINATES

x/c	z/c, upper	z/c, lower
0.00000	0.00000	0.00000
.00200	.01040	-.00500
.00500	.01590	-.00940
.01250	.02440	-.01450
.02500	.03420	-.01910
.03750	.04180	-.02280
.05000	.04760	-.02550
.07500	.05640	-.02990
.10000	.06290	-.03330
.12500	.06800	-.03600
.15000	.07220	-.03820
.17500	.07560	-.04000
.20000	.07830	-.04150
.22500	.08050	-.04270
.25000	.08220	-.04360
.27500	.08350	-.04430
.30000	.08440	-.04480
.32500	.08490	-.04510
.35000	.08500	-.04520
.37500	.08470	-.04500
.40000	.08410	-.04470
.42500	.08320	-.04420
.45000	.08200	-.04350
.47500	.08050	-.04260
.50000	.07870	-.04150
.52500	.07660	-.04010
.55000	.07420	-.03850
.57500	.07150	-.03660
.60000	.06850	-.03440
.62500	.06530	-.03190
.65000	.06180	-.02910
.67500	.05810	-.02620
.70000	.05420	-.02320
.72500	.05010	-.02020
.75000	.04580	-.01720
.77500	.04140	-.01420
.80000	.03680	-.01120
.82500	.03210	-.00840
.85000	.02730	-.00590
.87500	.02240	-.00390
.90000	.01740	-.00260
.92500	.01230	-.00210
.95000	.00700	-.00280
.97500	.00150	-.00510
1.00000	-.00430	-.00940

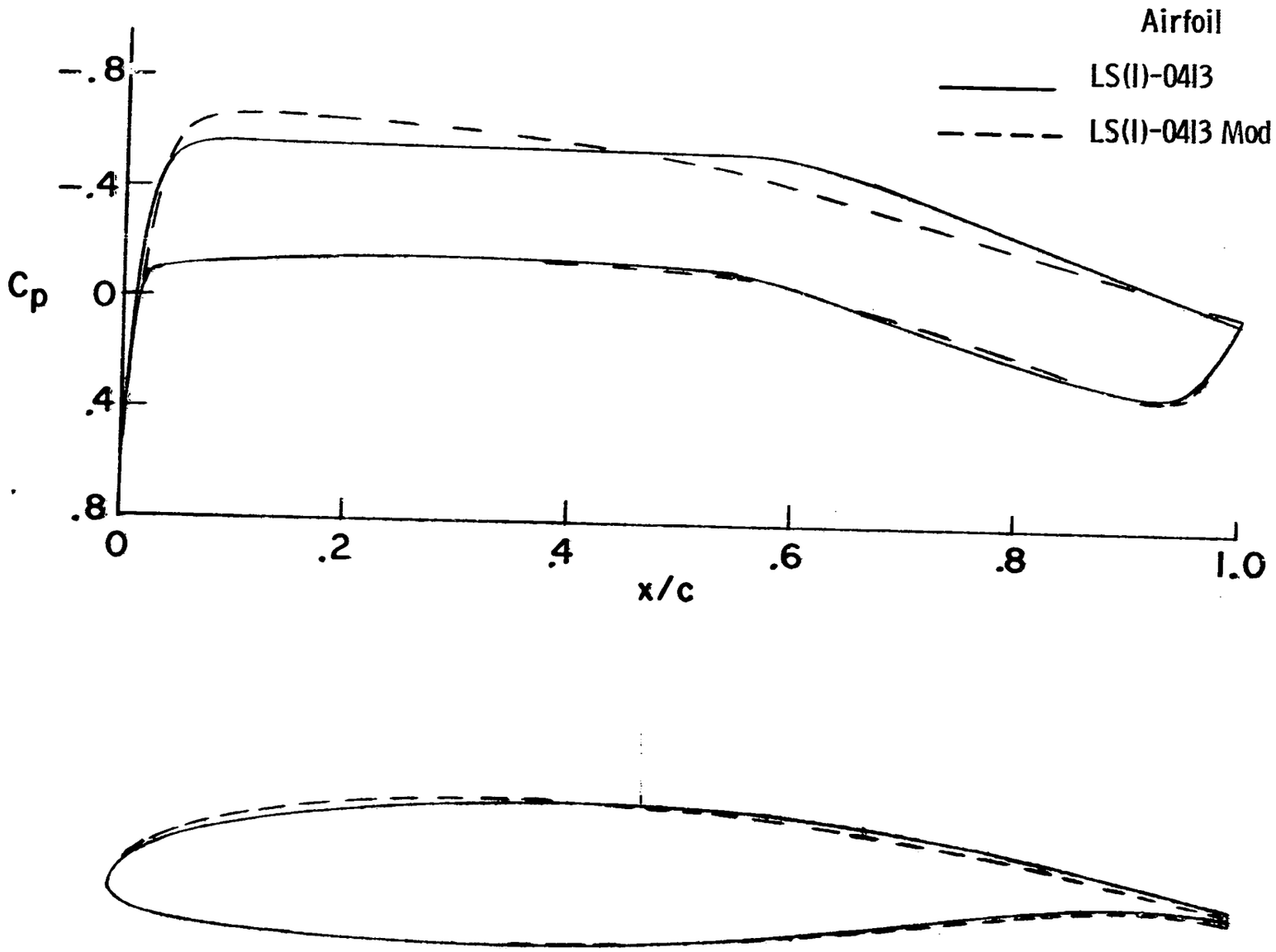

Figure 1.- Comparison of chordwise pressure distributions and section shapes for LS(1)-0413 and LS(1)-0413 Mod airfoils at $c_l \approx 0.40$.

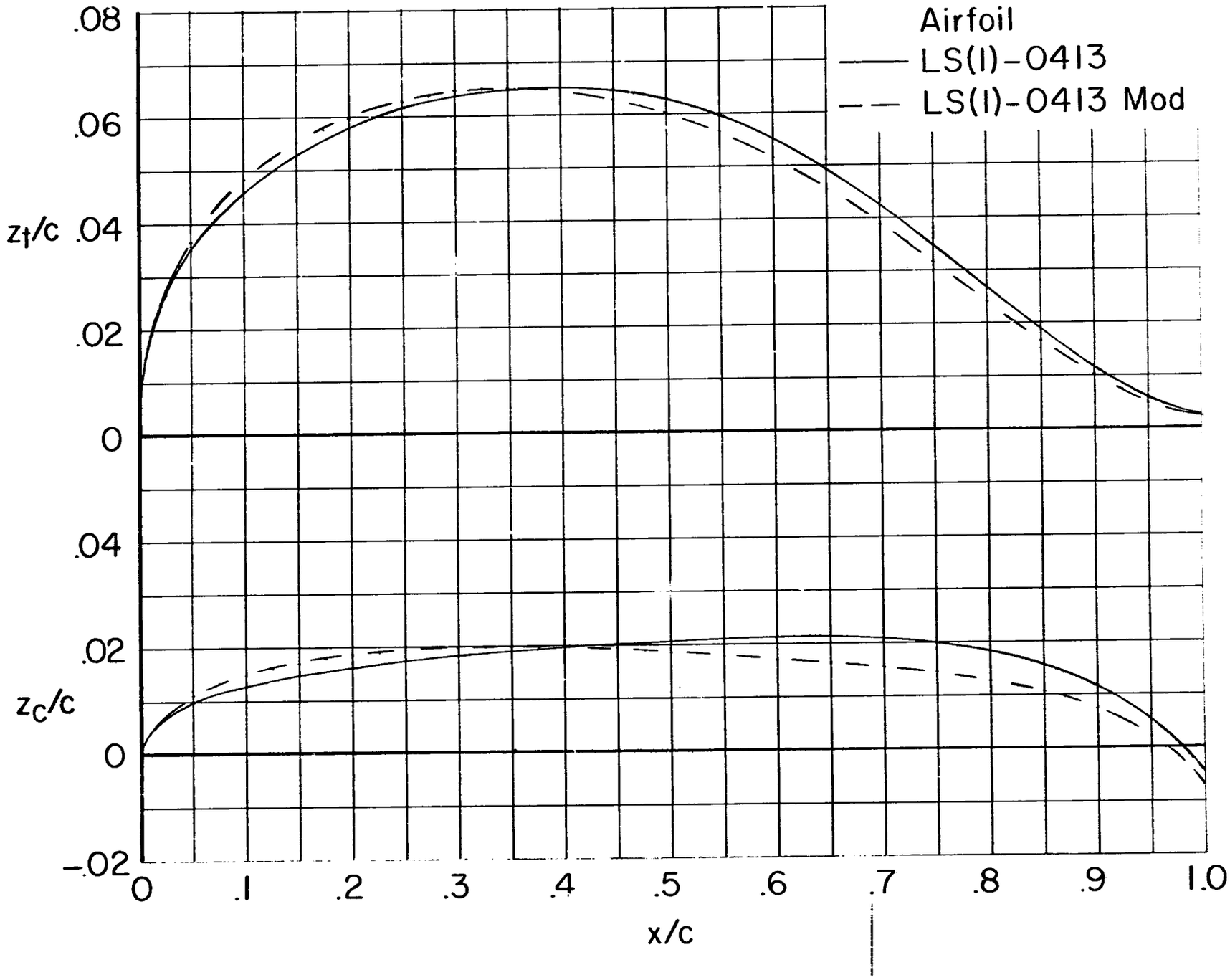

Figure 2.- Comparison of mean thickness distributions and camber lines for LS(1)-0413 and LS(1)-0413 Mod airfoils.

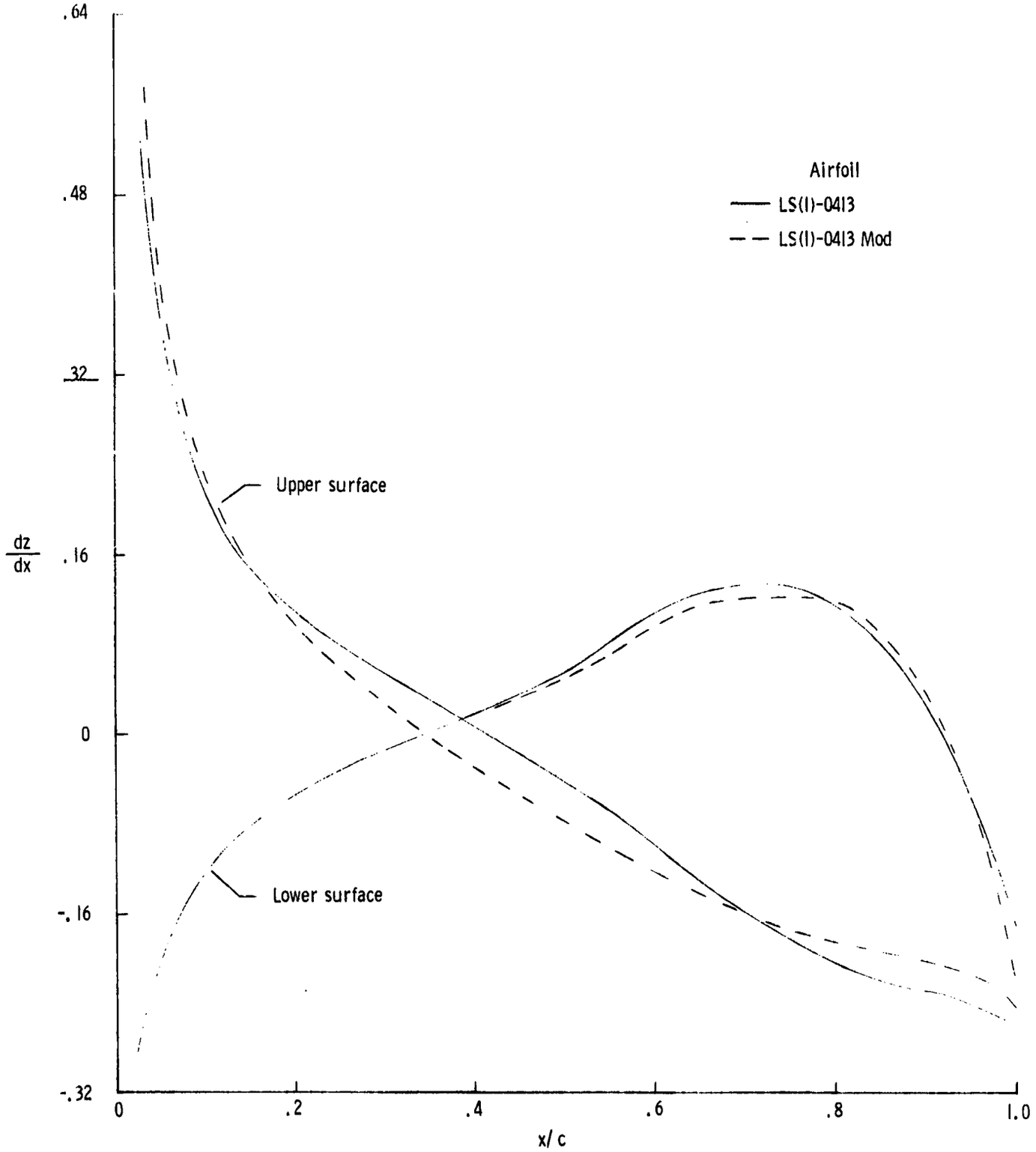

Figure 3.- Chordwise distribution of slopes.

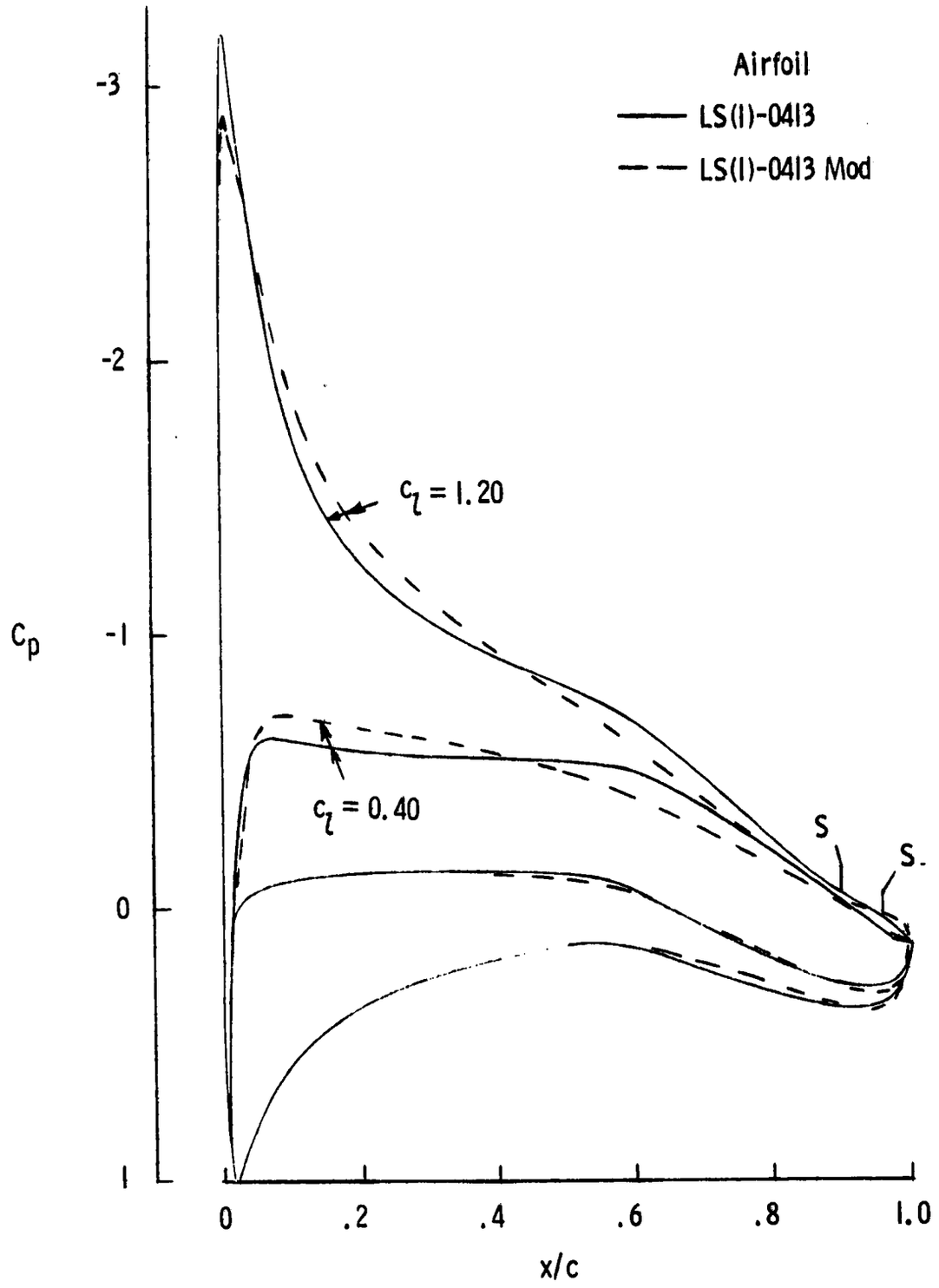

(a) $R = 2.0 \times 10^6$.

Figure 4.- Theoretical chordwise pressure distributions for LS(1)-0413 and LS(1)-0413 Mod airfoils at M = 0.15.

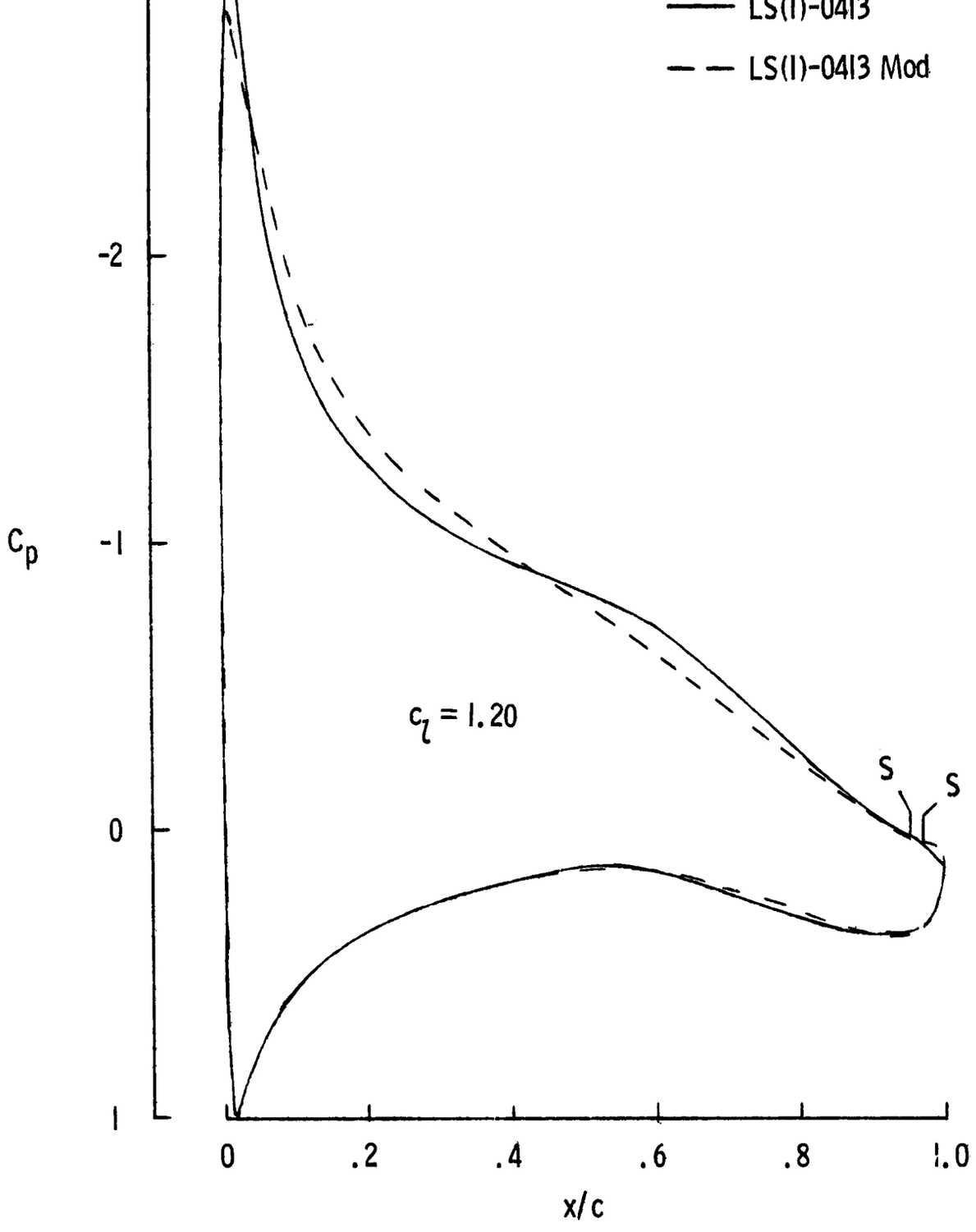

(b) $R = 4.0 \times 10^6$; $c_l = 1.2$.

Figure 4.- Concluded.

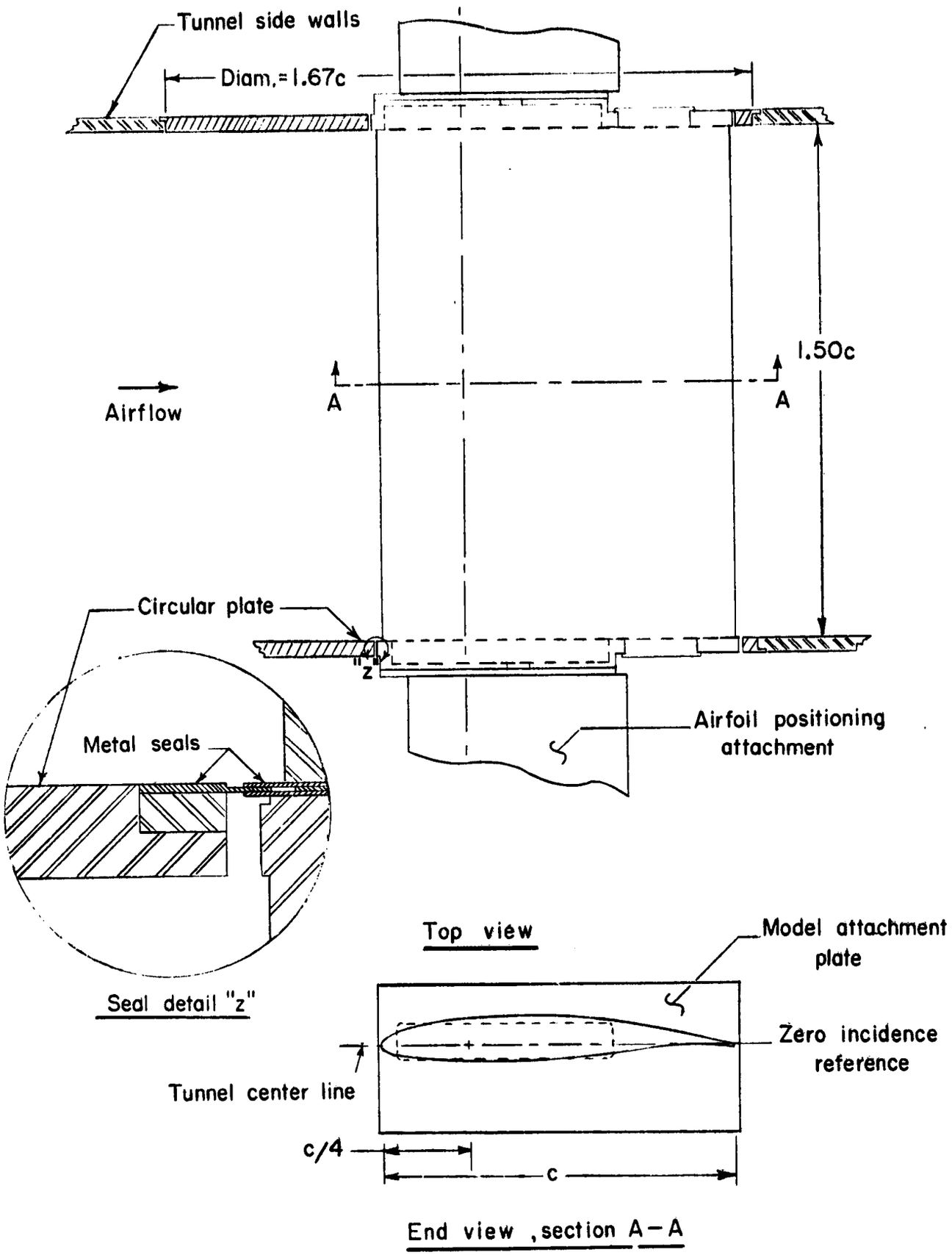

Figure 5.- Airfoil model mounted in wind tunnel. c = 61 cm (24 in.).

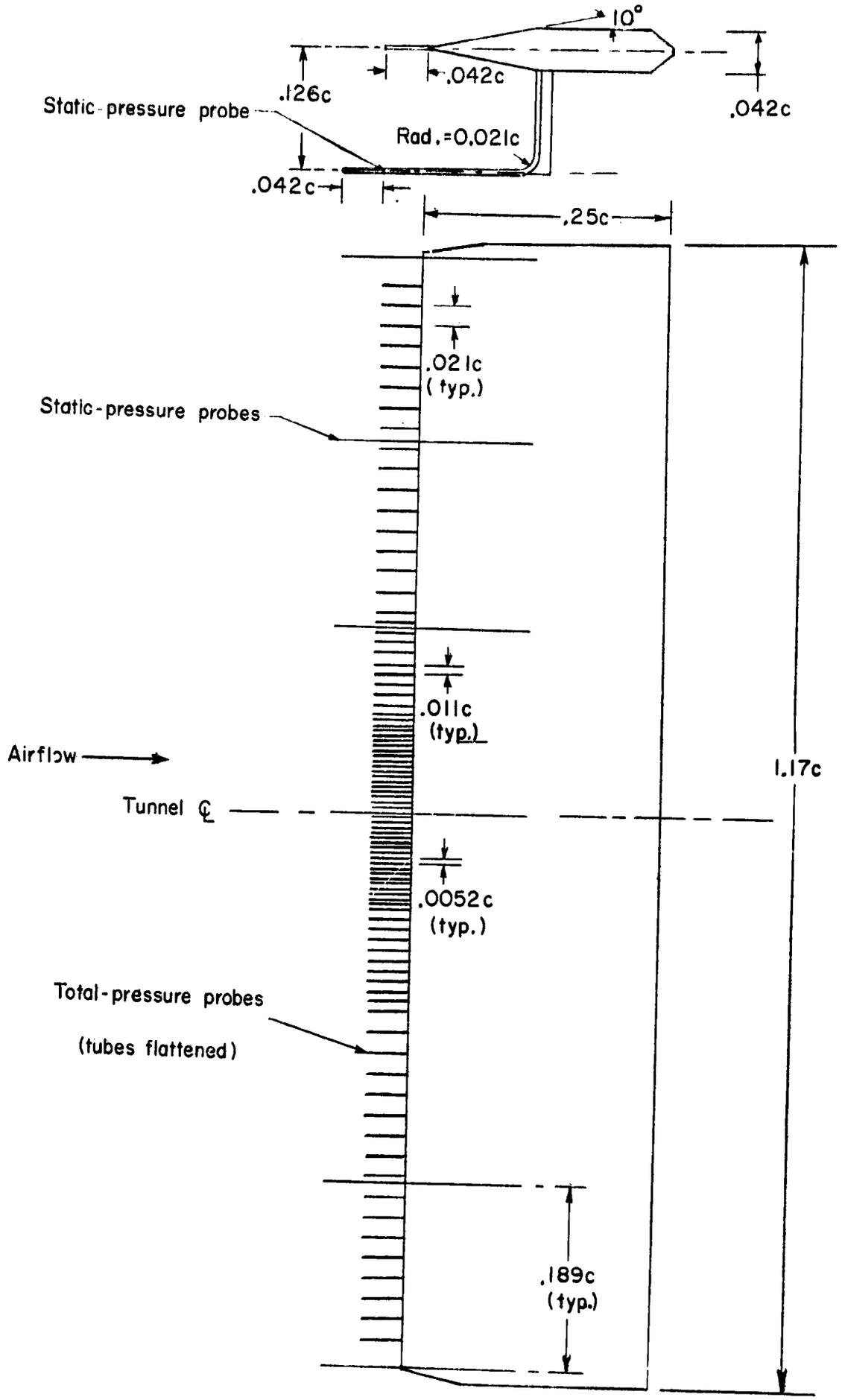

Figure 6. - Wake survey rake. c = 61 cm (24 in.).

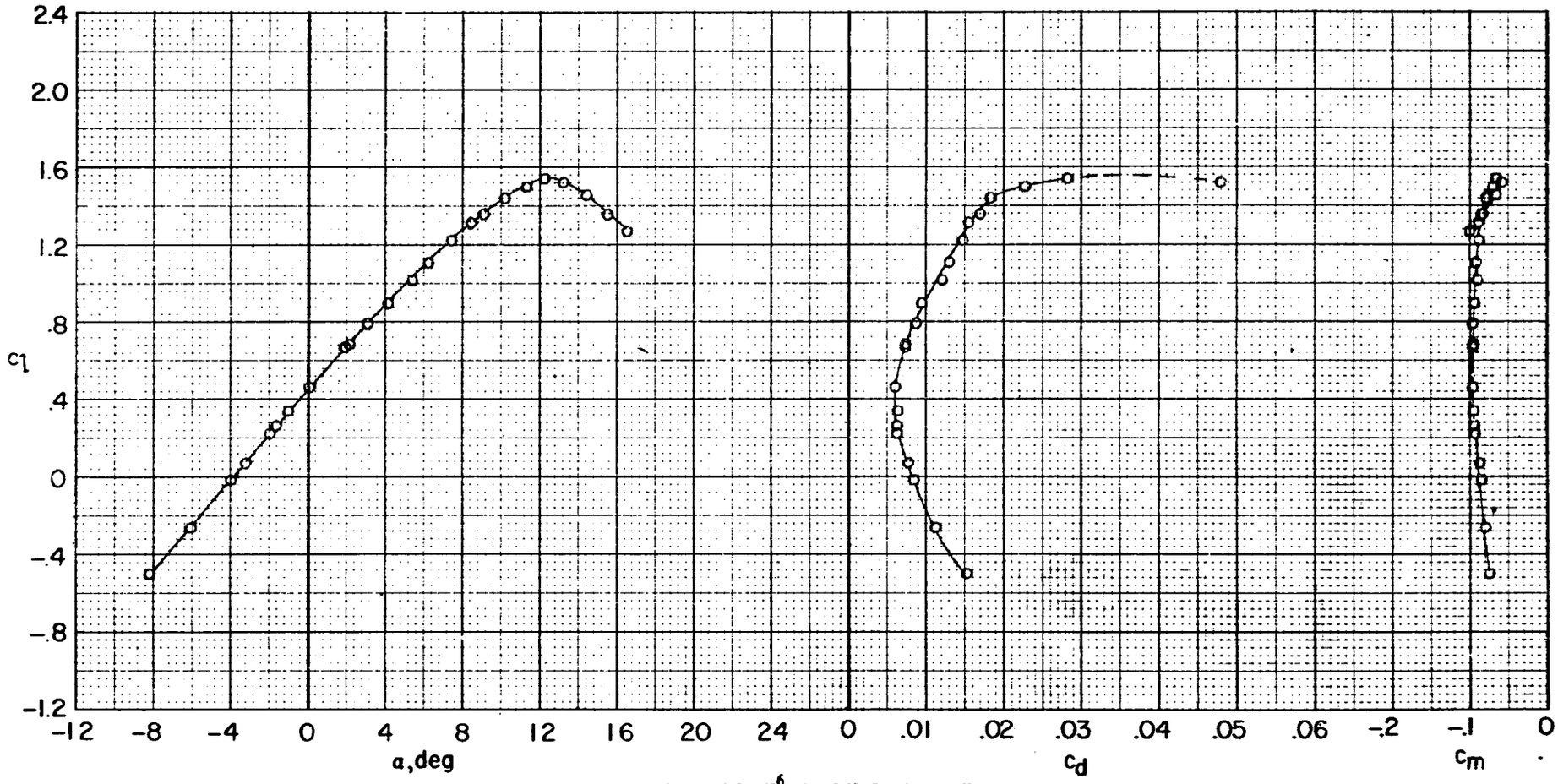

(a) R = 1.0 x 10^6; M = 0.10; Roughness off.

Figure 7.- Effect of Reynolds number on section characteristics for LS(1)-0413 Mod airfoil.

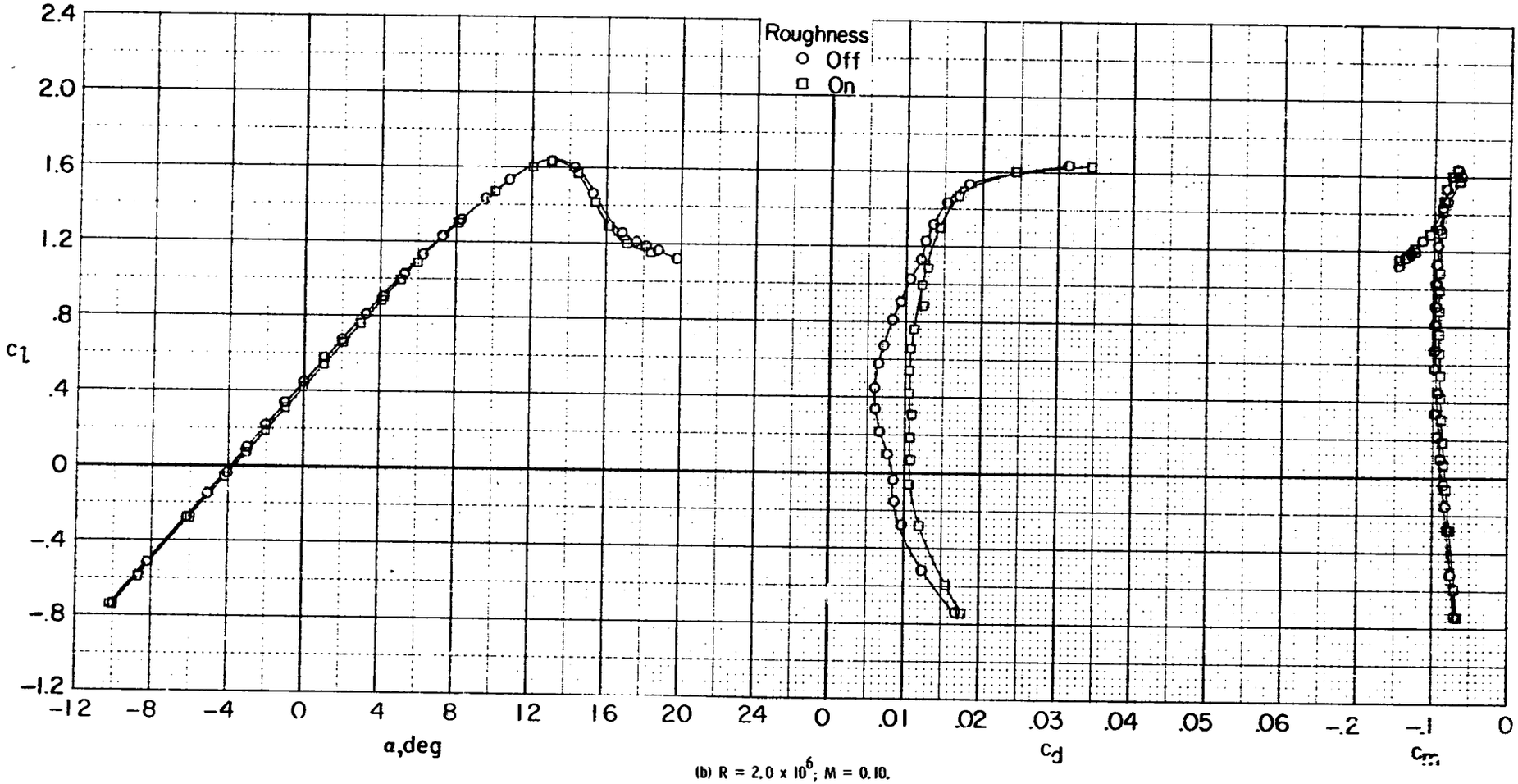

(b) R = 2.0 x 10^6; M = 0.10.

Figure 7.- Continued.

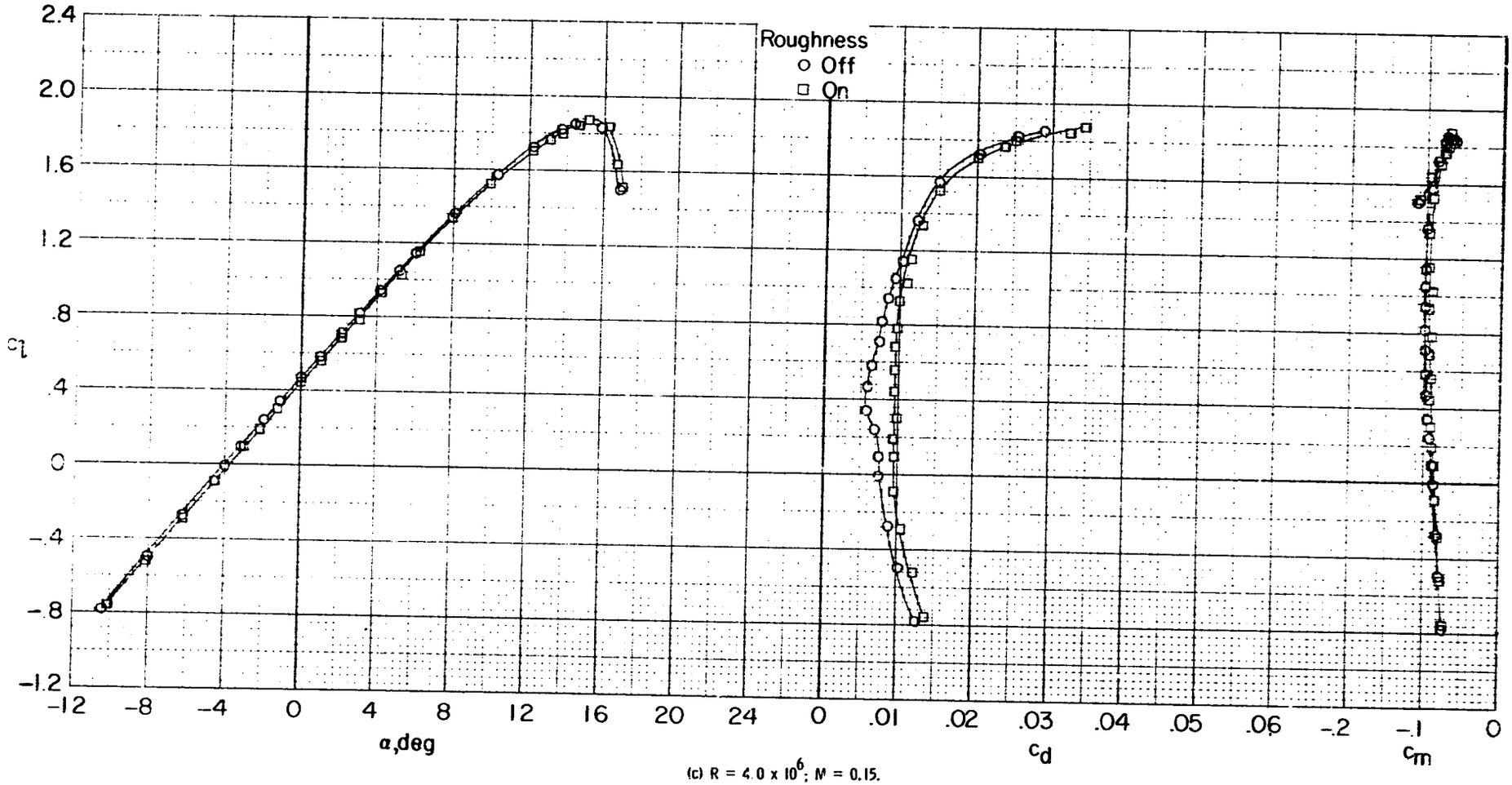

(c) R = 4.0 x 10^6; M = 0.15.

Figure 7. - Continued.

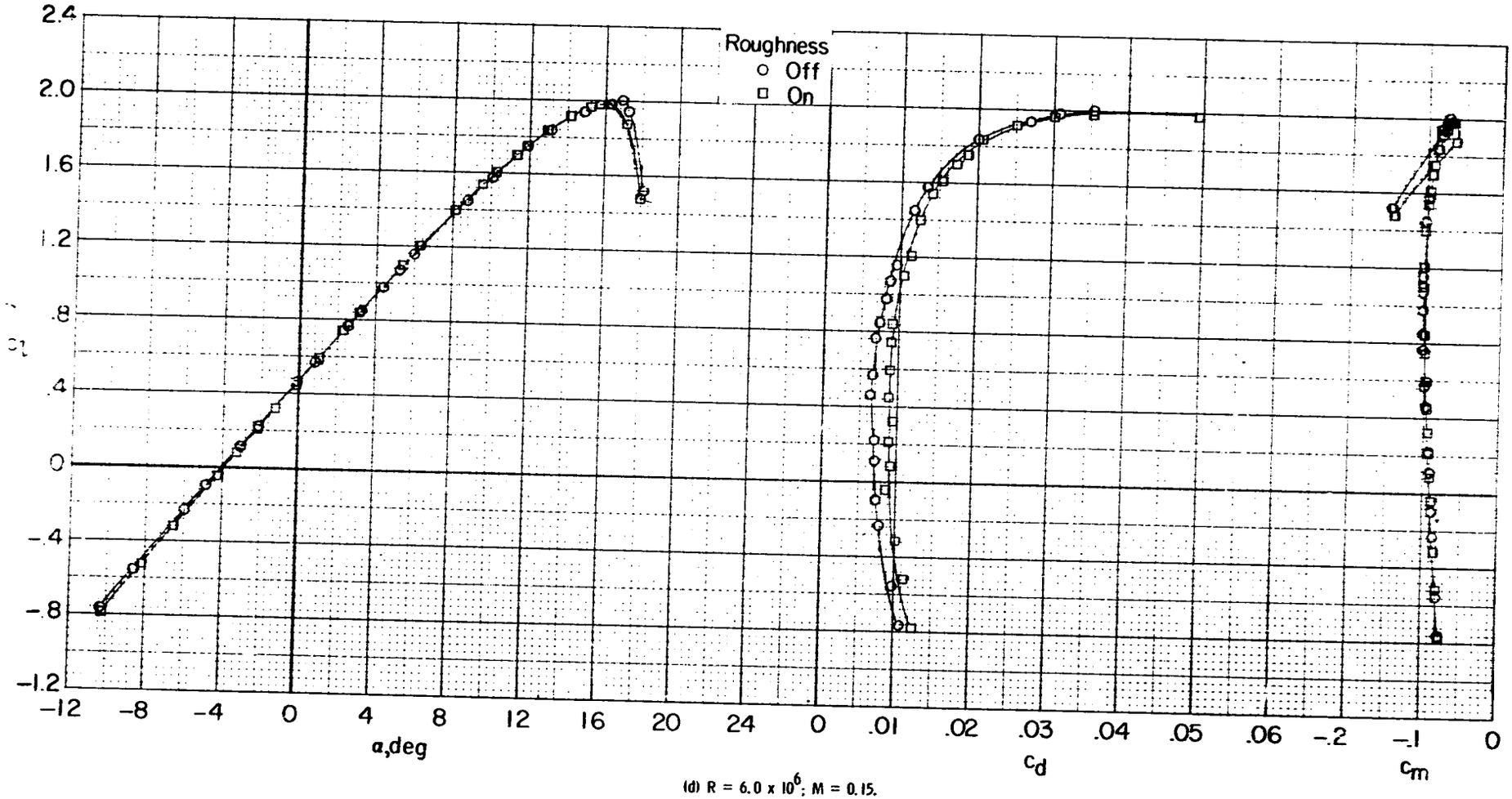

(d) R = 6.0 x 10^6; M = 0.15.

Figure 7.- Continued.

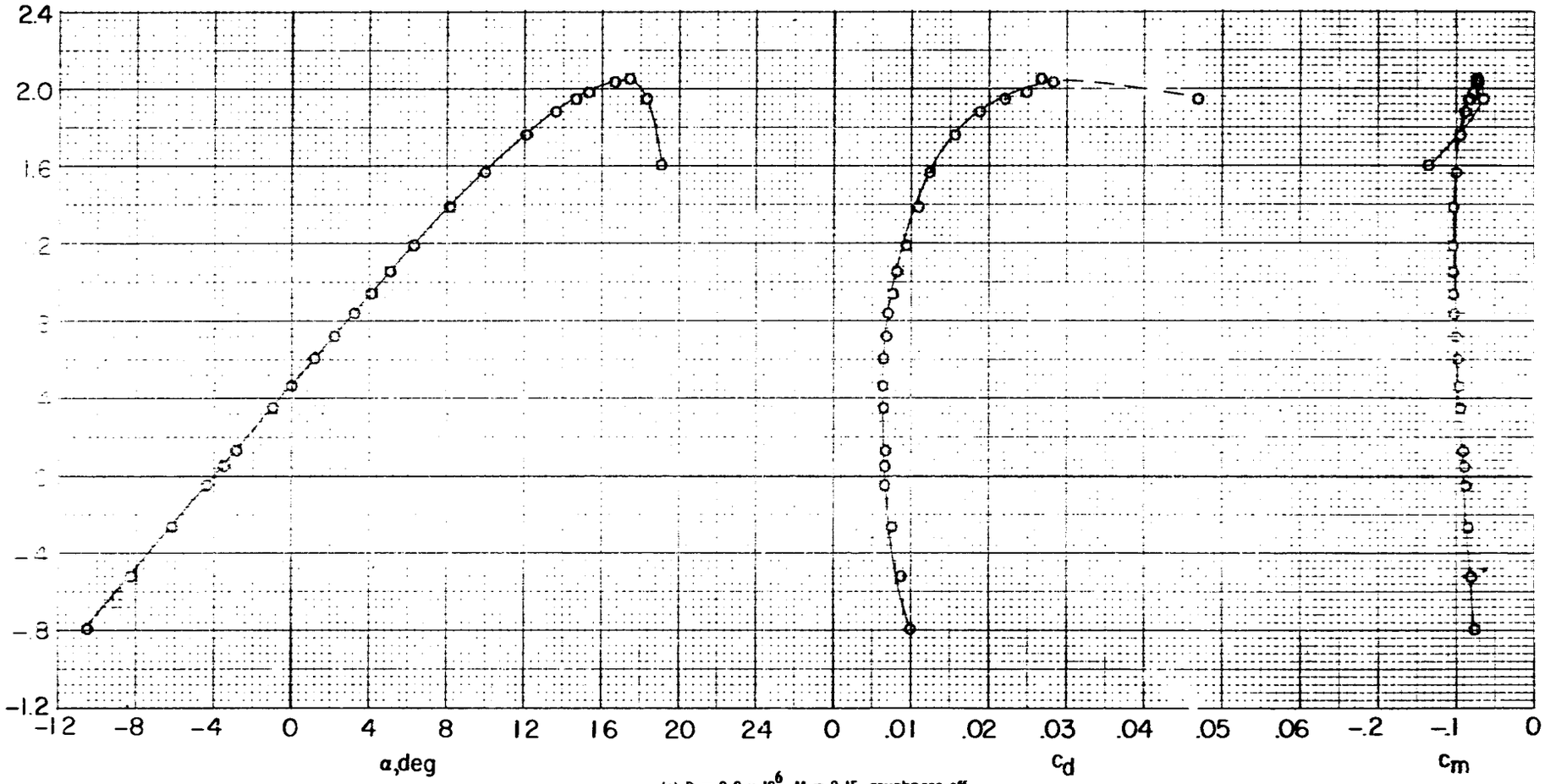

(e) R = 9.0 x 10^6; M = 0.15; roughness off.

Figure 7.- Concluded.

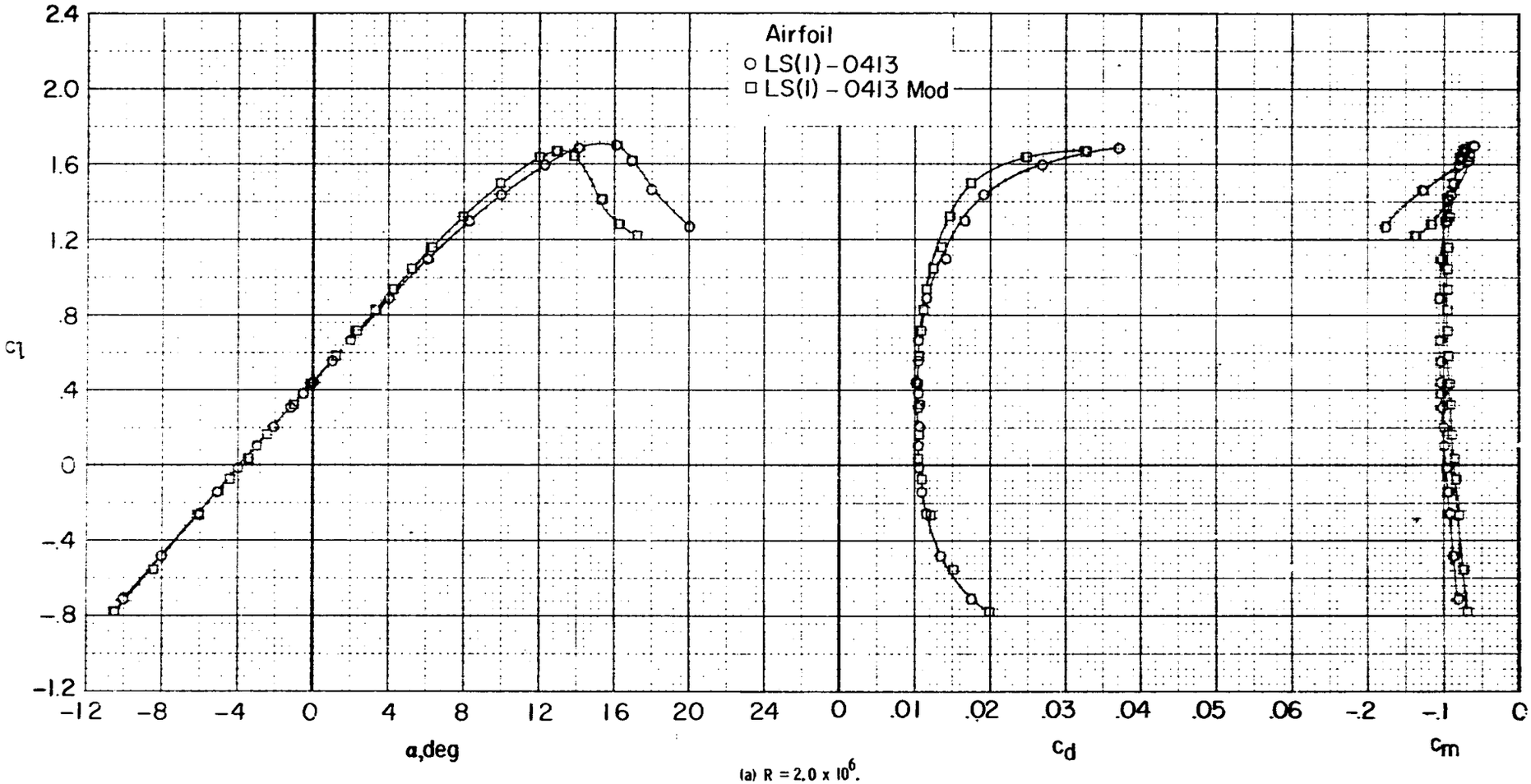

(a) R = 2.0 x 10^6.

Figure 8.- Comparison of section characteristics for LS(1)-0413 and LS(1)-0413 Mod airfoils for M = 0.15 and roughness on.

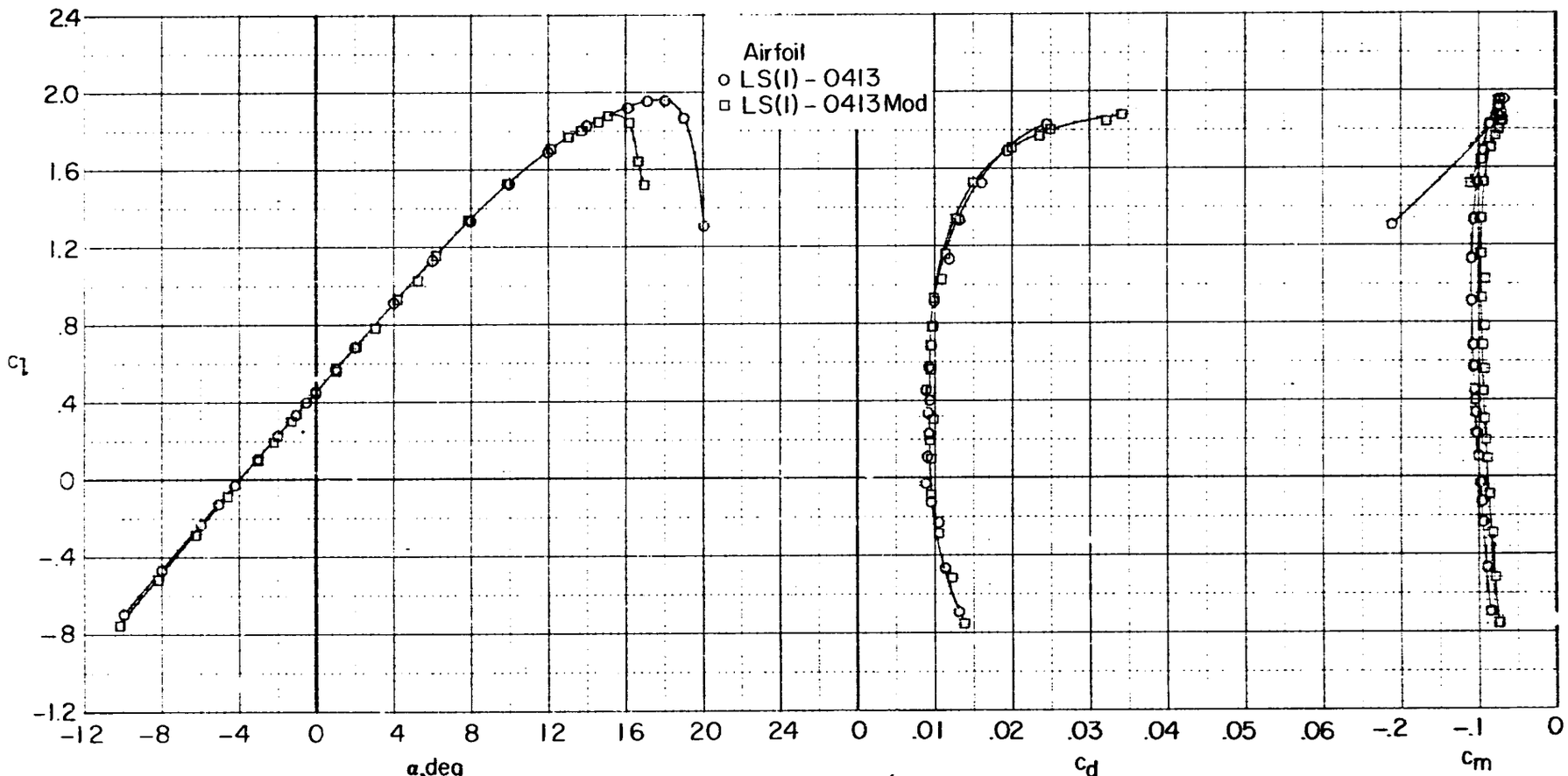

(b) $R = 4.0 \times 10^6$.

Figure 8. - Continued.

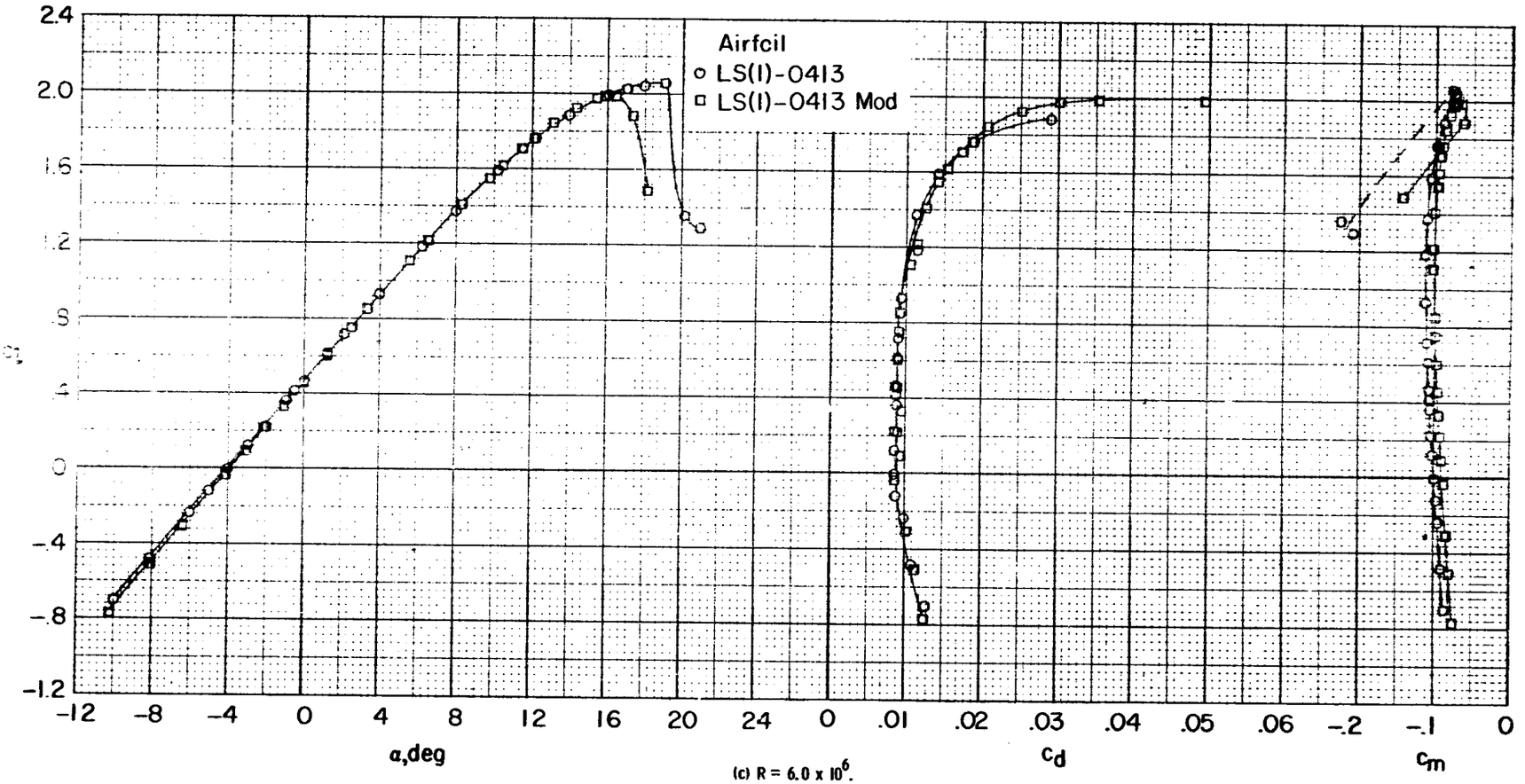

(c) R = 6.0 x 10^6.

Figure 8. - Concluded.

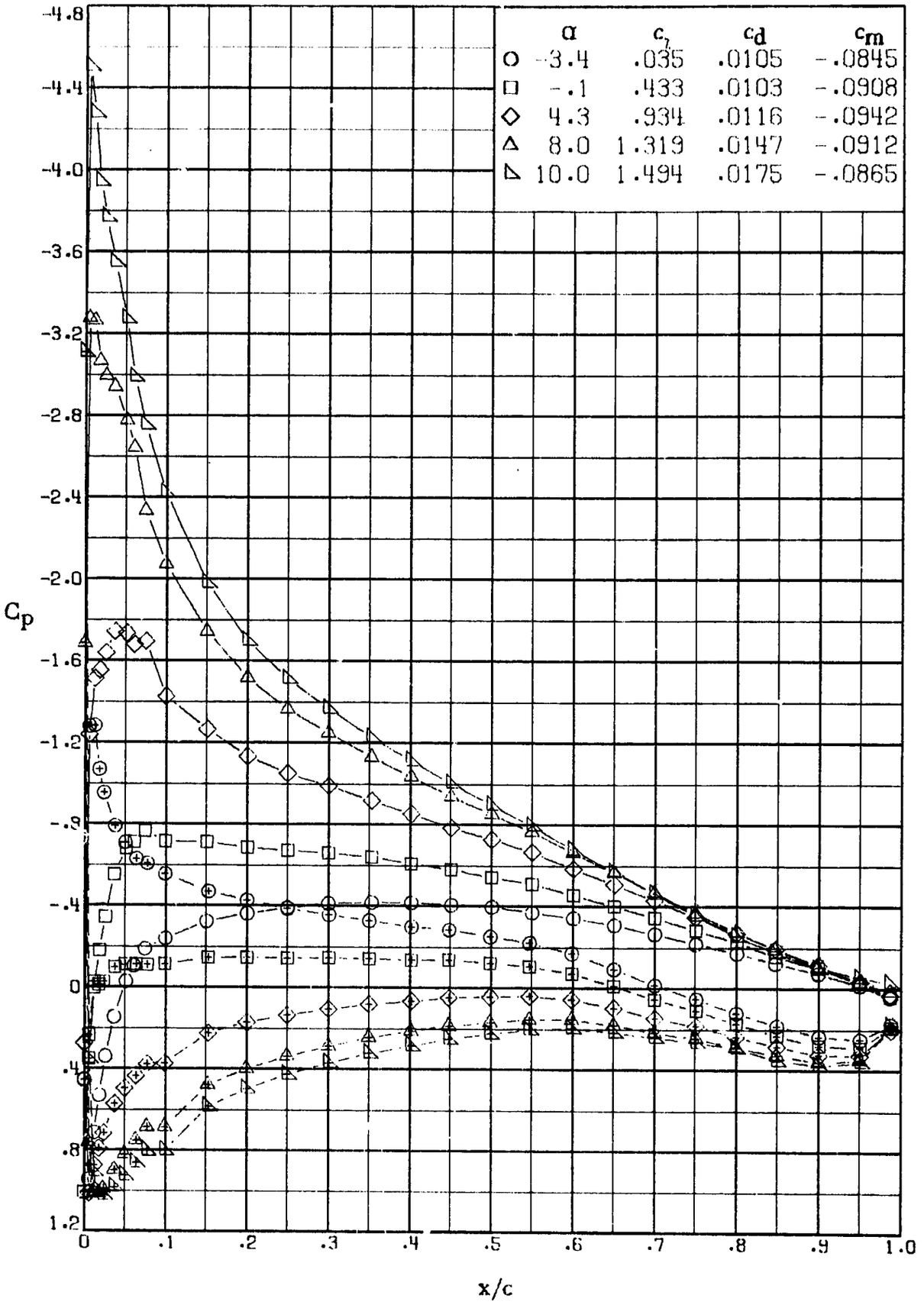

(a) $R = 2.0 \times 10^6$.

Figure 9. Effect of Reynolds number on chordwise pressure distributions for LS(1)-0413 Mod airfoil for M = 0.15 and roughness on. (Centered symbols lower surface).

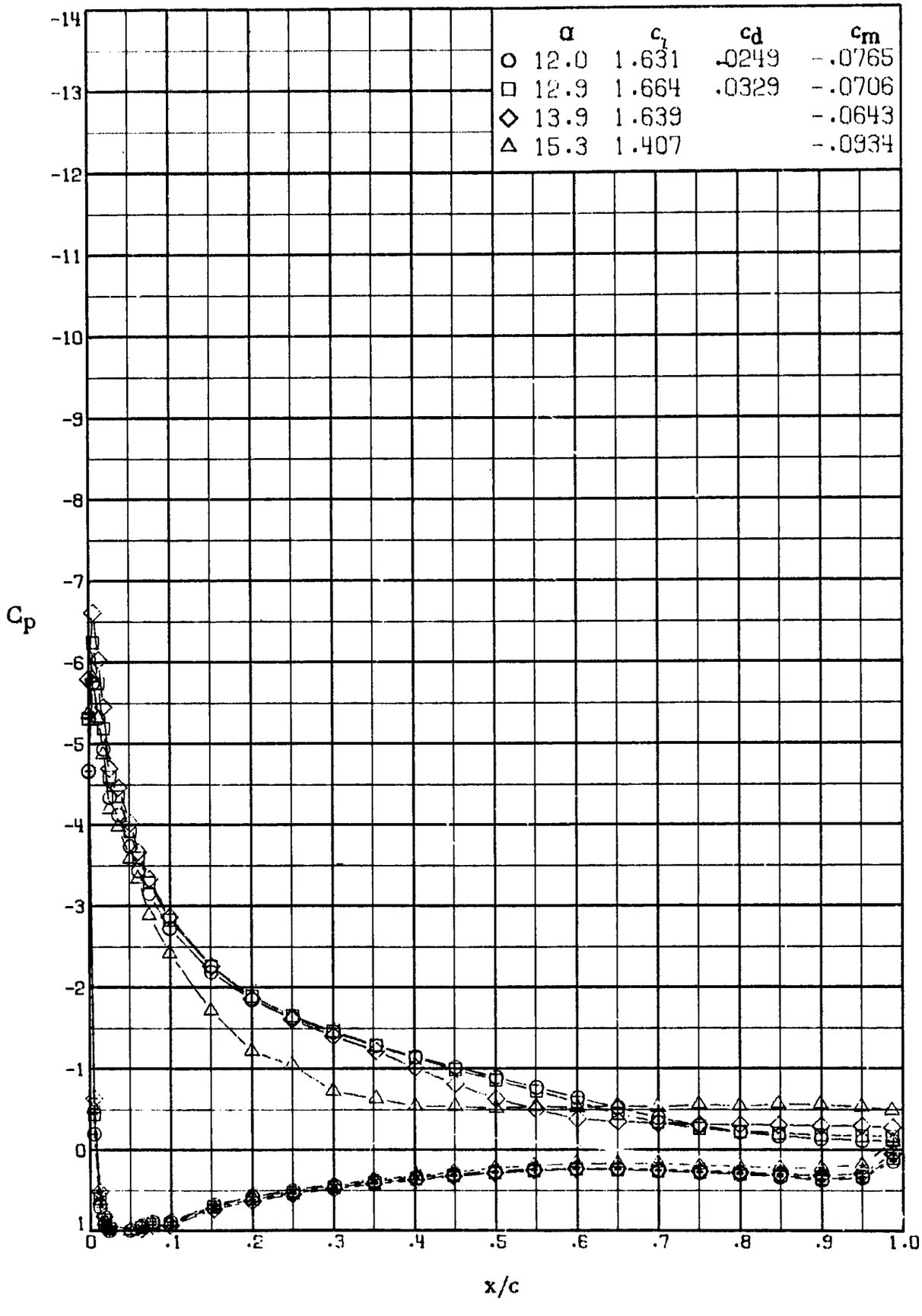

(a) R = 2.0 x 10^6. Concluded.

Figure 9. - Continued.

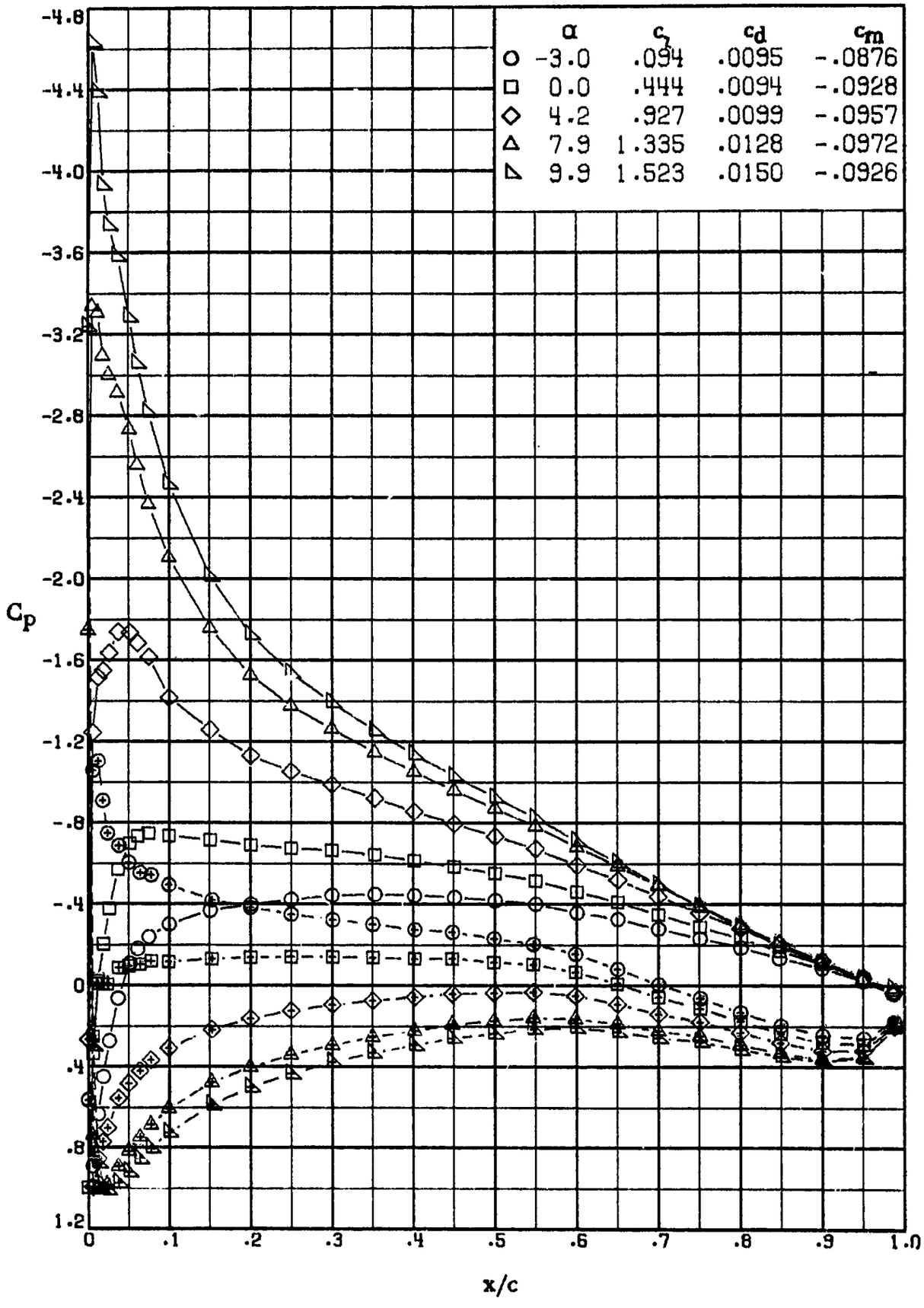

(b) R = 4.0 x 10^6.

Figure 9. - Continued

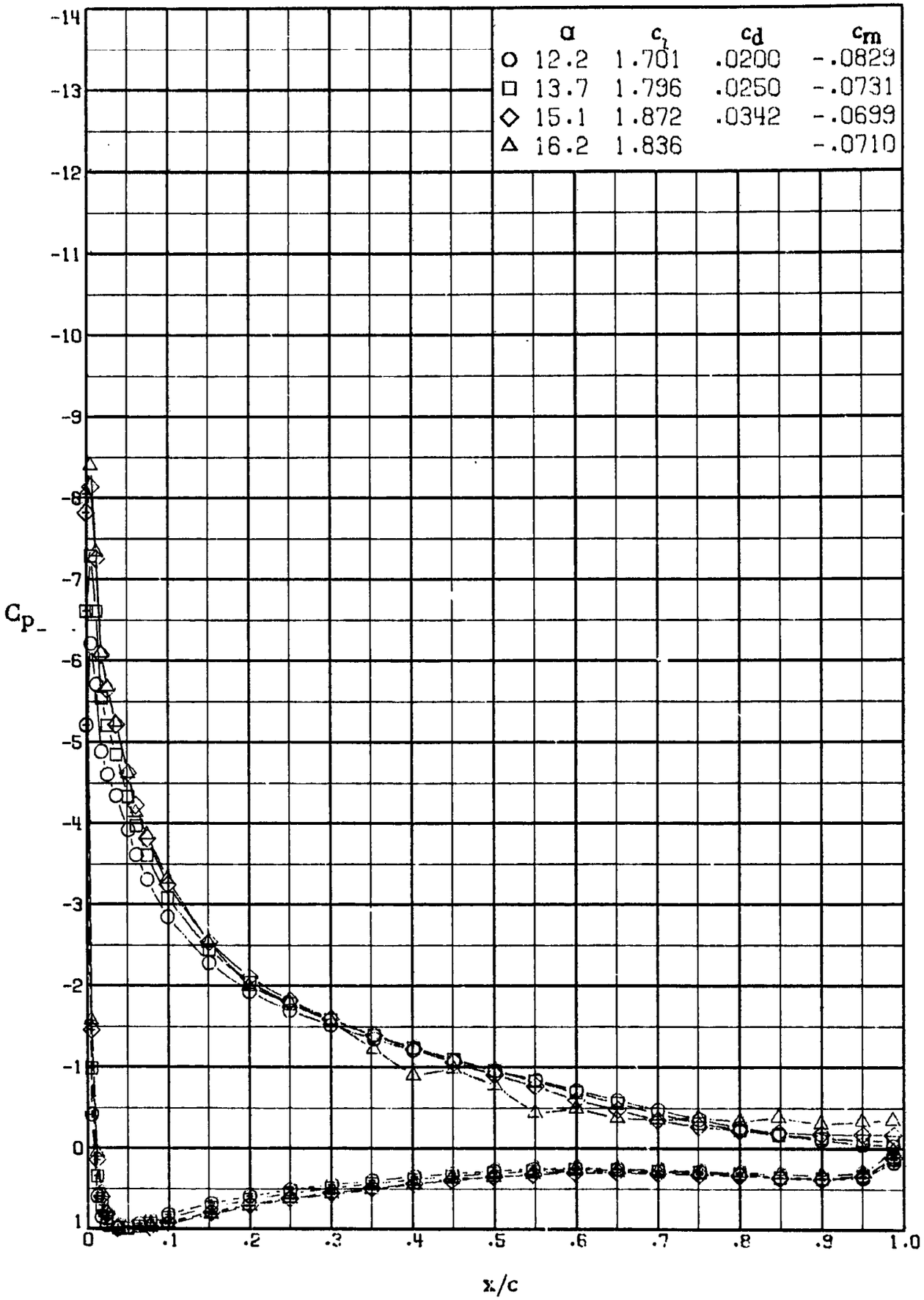

(b) R = 4.0×10^6. Concluded.

Figure 9. - Continued.

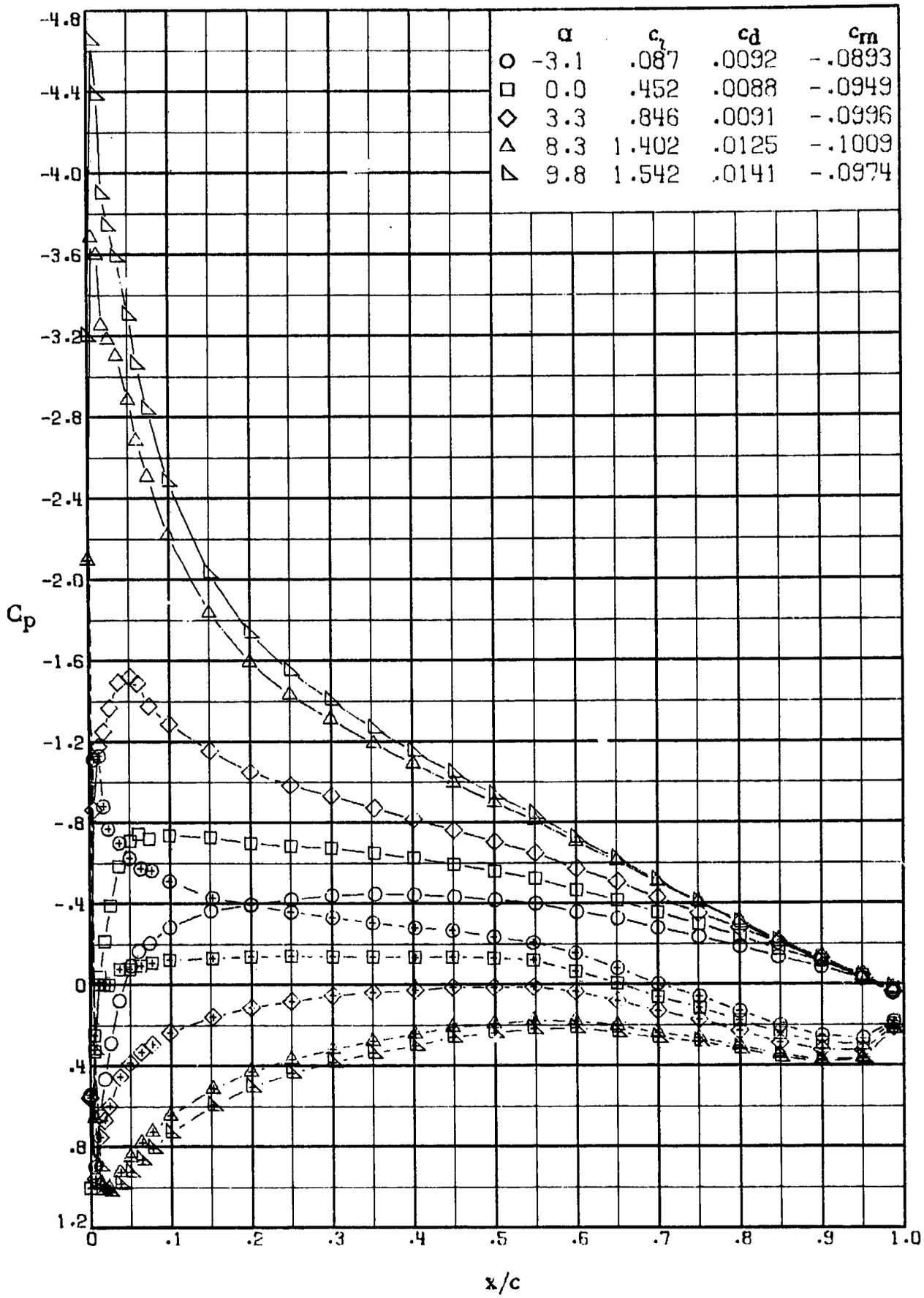

(c) R = 6.0 x 10^6.

Figure 9.- Continued.

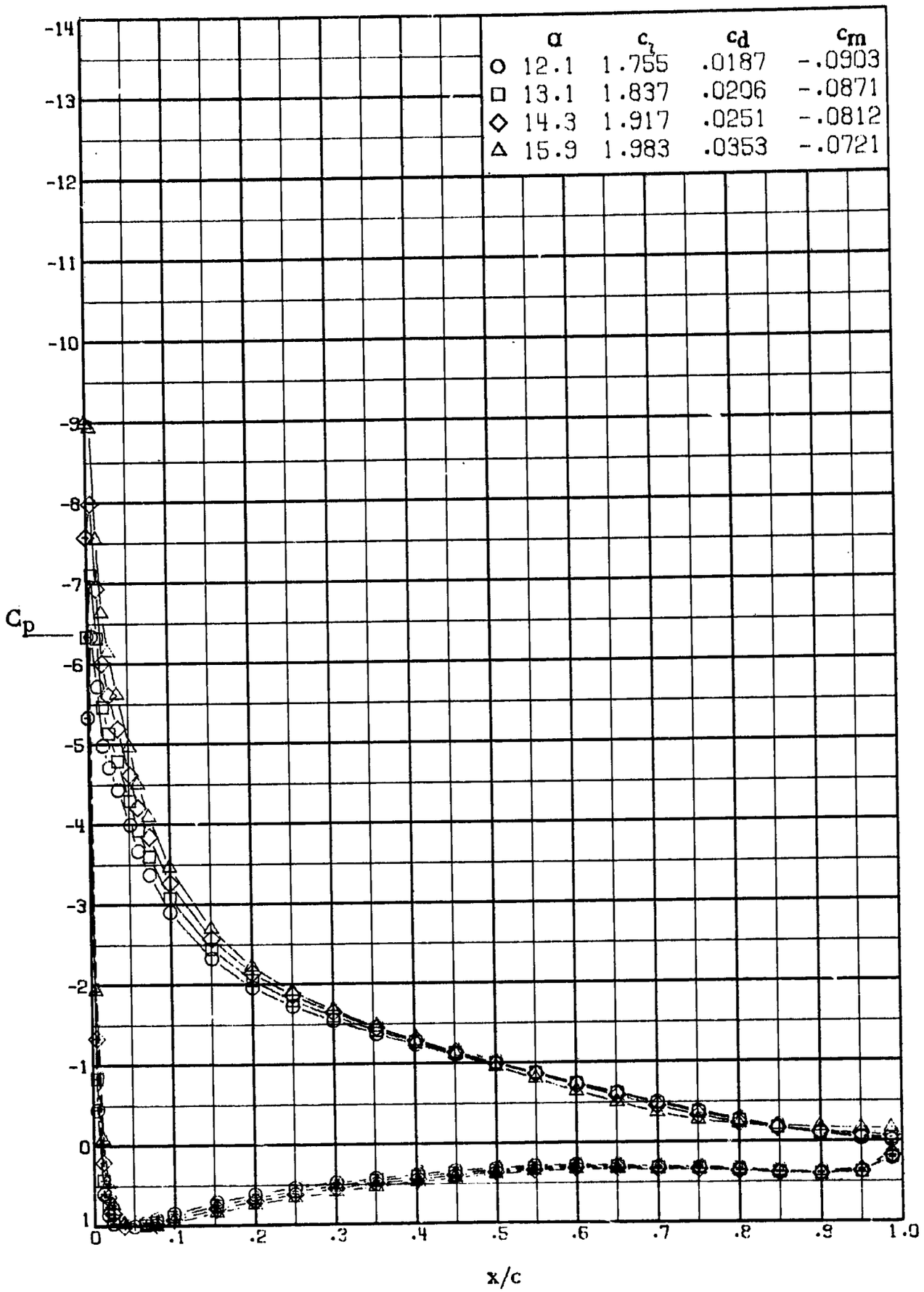

(c) R = 6.0 x 10^6. Concluded.

Figure 9.- Concluded.

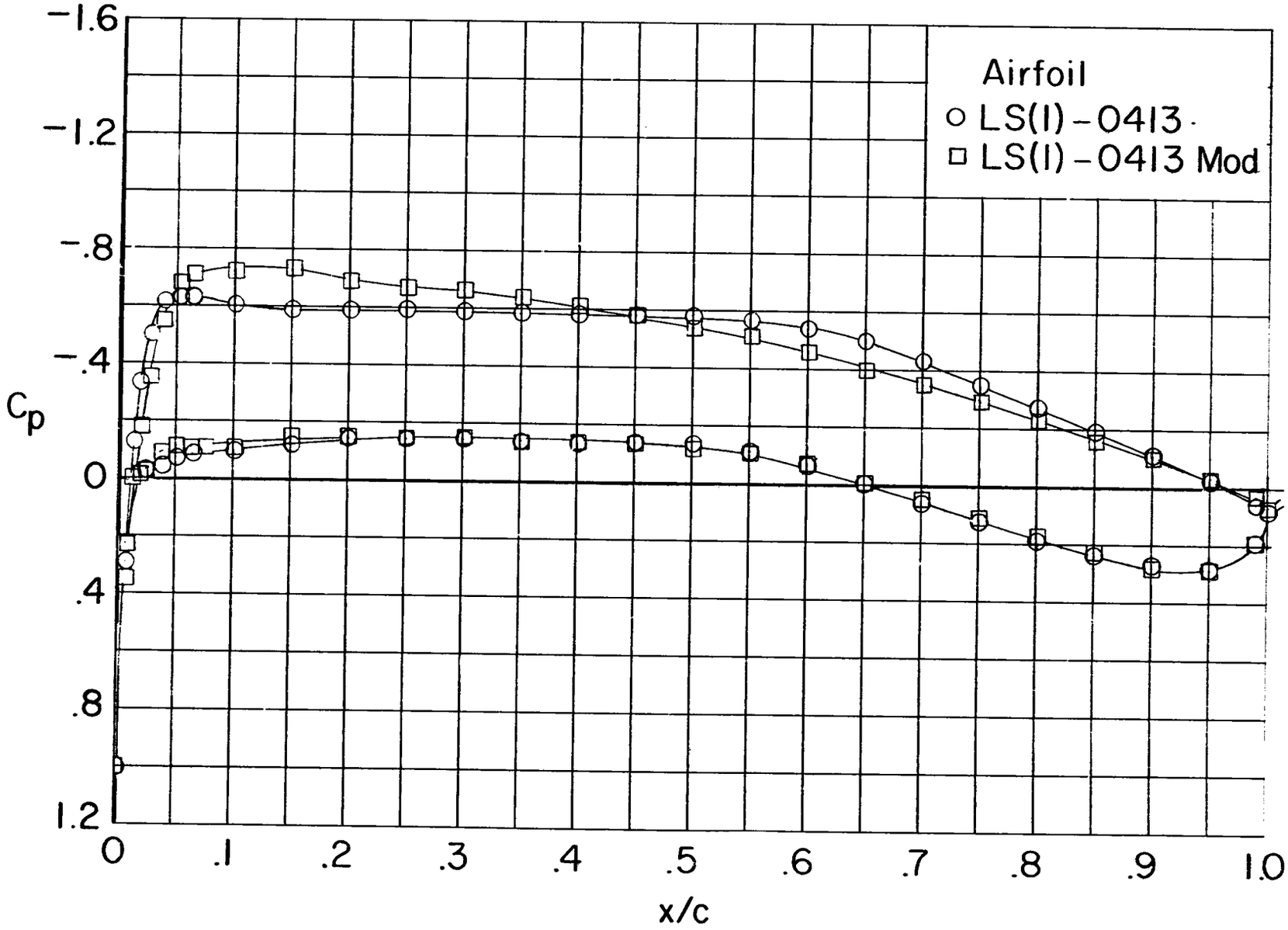

(a) $\alpha \approx 0^0$; $R \approx 2.0 \times 10^6$.

Figure 10.- Comparison of chordwise pressure distributions for LS(1)-0413 and LS(1)-0413 Mod airfoils for M = 0.15 and roughness on. (Flagged symbols indicate base pressure orifice).

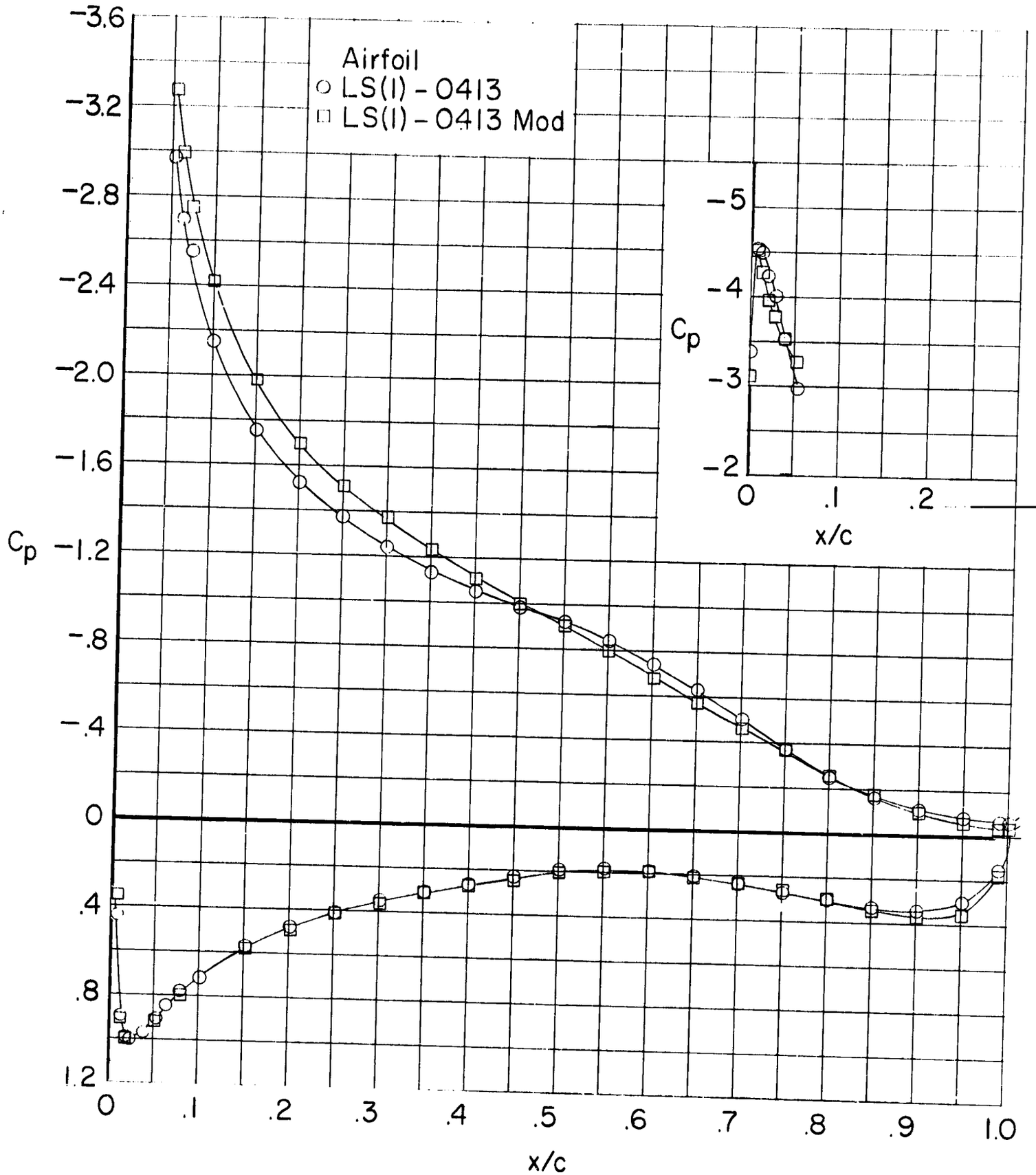

(b) $\alpha \approx 10^0$; $R \approx 2.0 \times 10^6$.

Figure 10. - Continued.

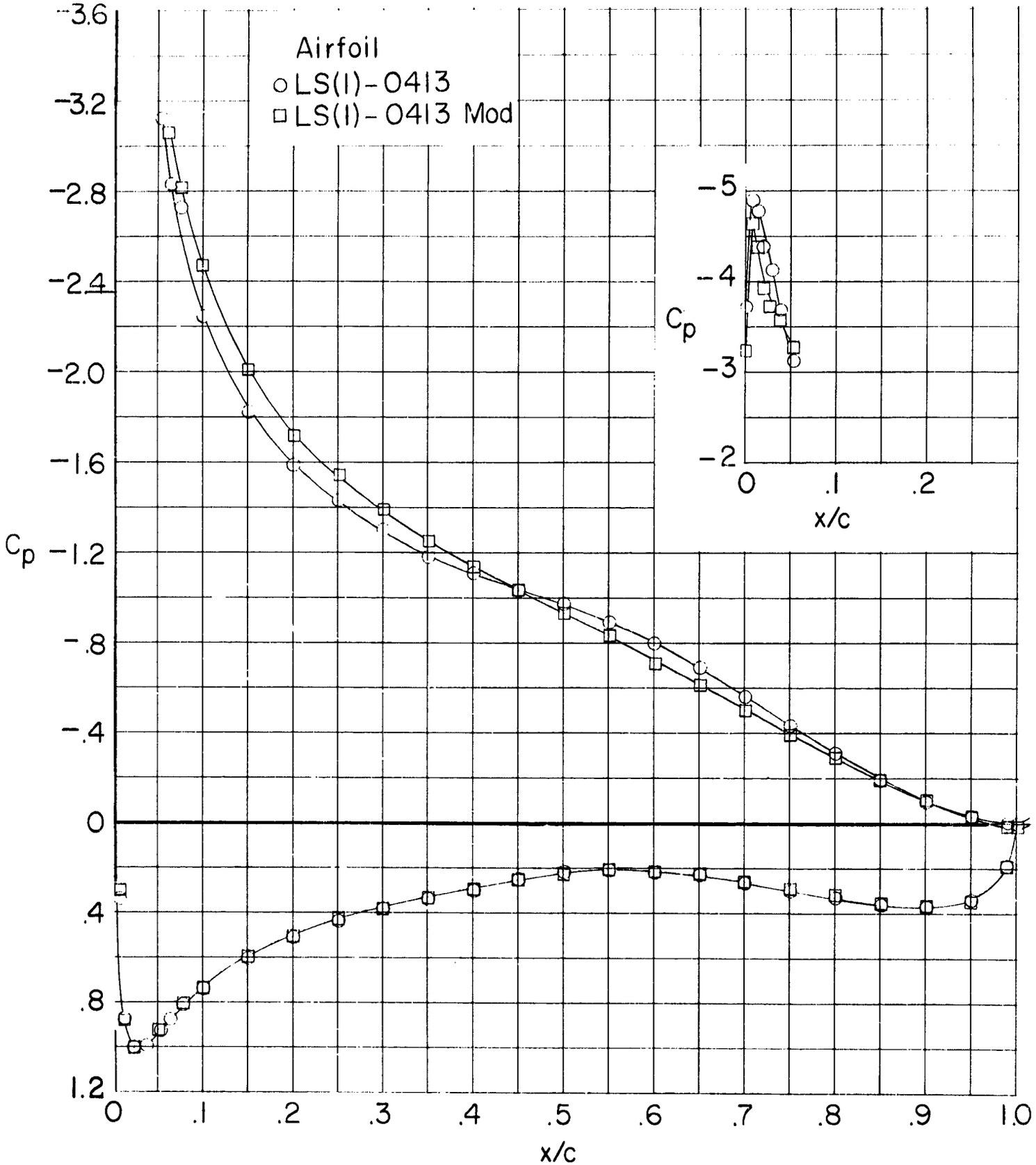

(c) $\alpha \approx 10^0$; $R \approx 4.0 \times 10^6$.

Figure 10. - Continued.

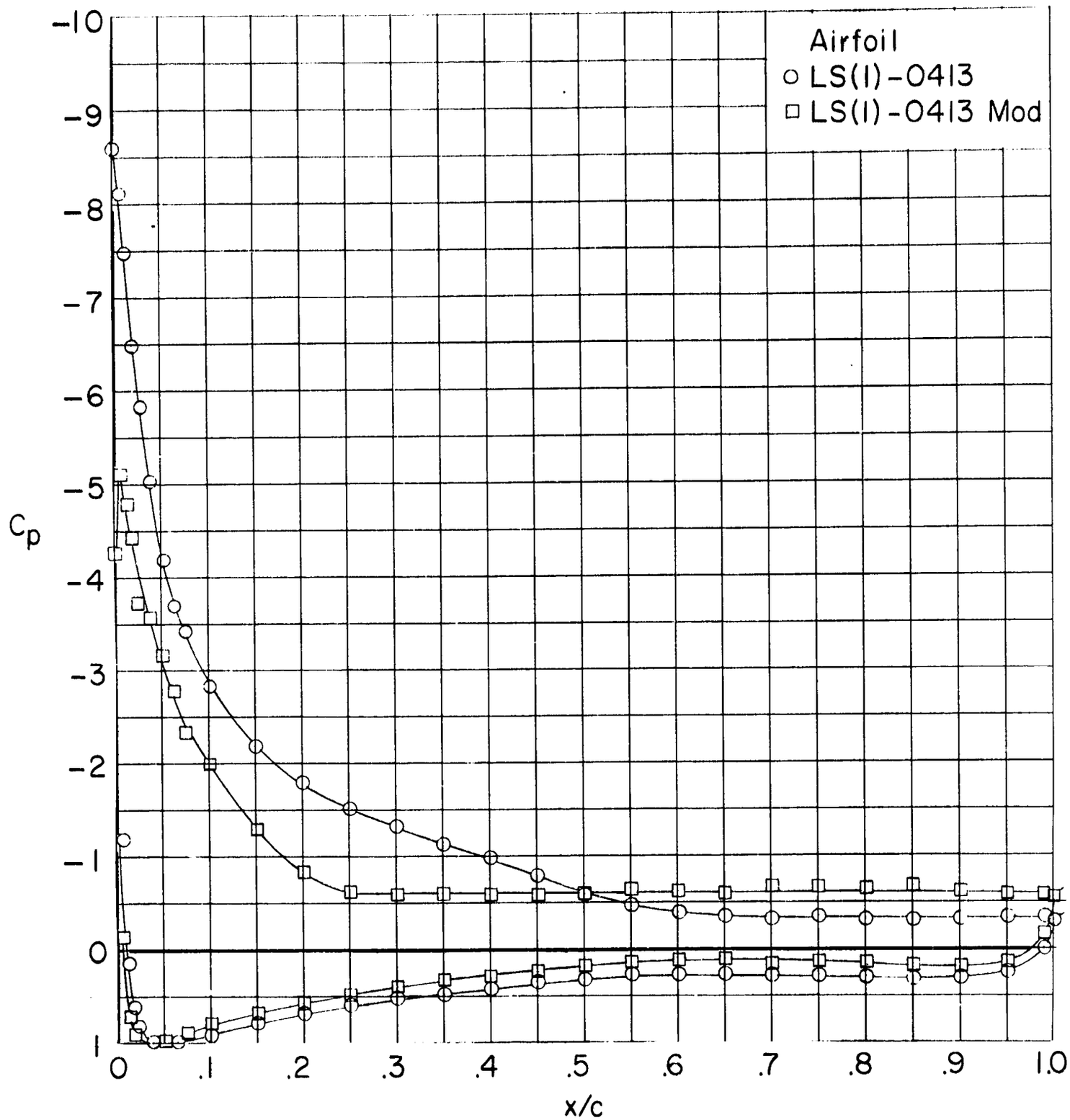

(d) $\alpha = 16^0$; $R \approx 2.0 \times 10^6$.

Figure 10. - Concluded.

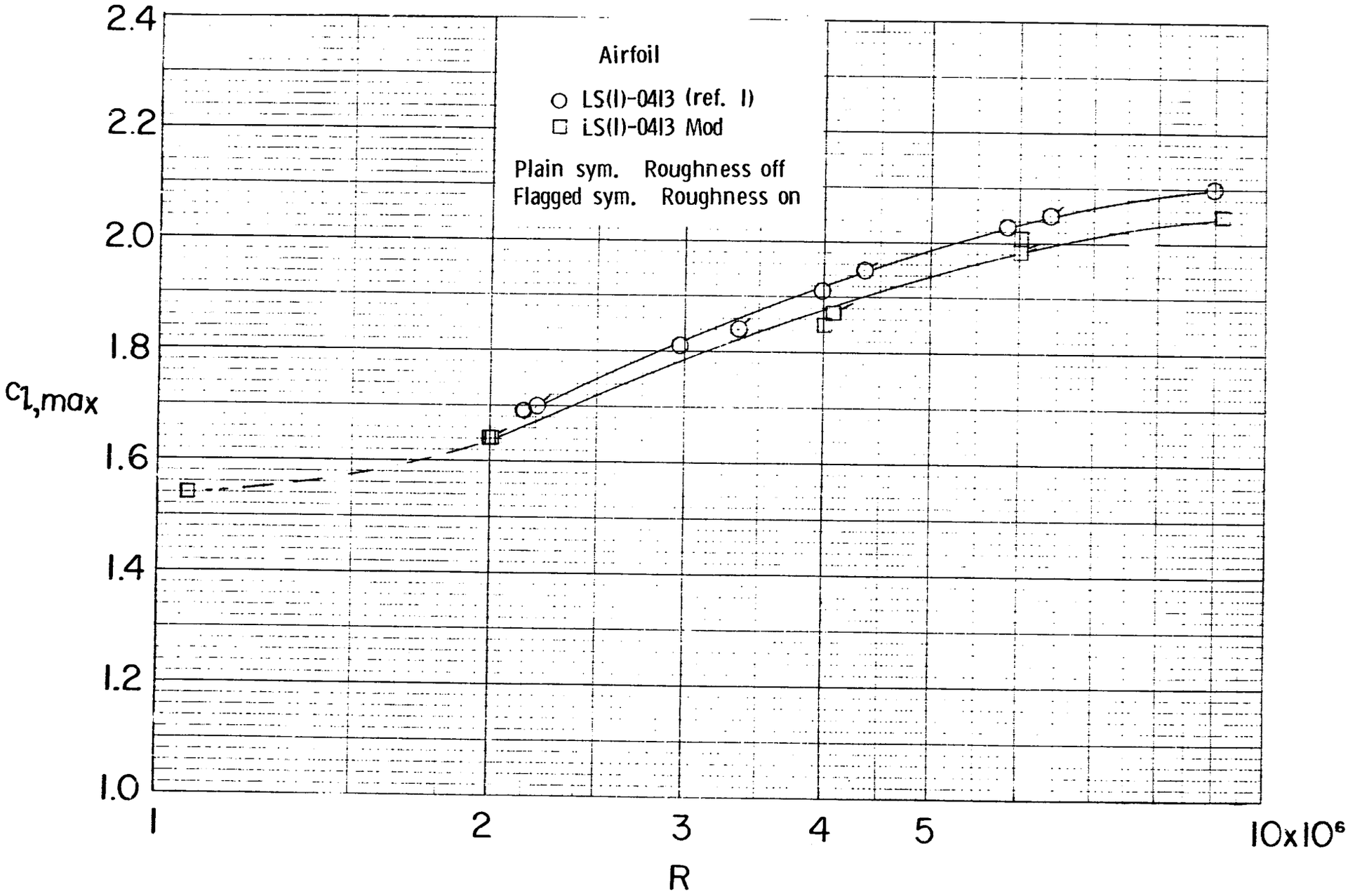

Figure 11. - Variation of maximum lift coefficient with Reynolds number for LS(1)-0413 and LS(1)-0413 Mod airfoils. $M \leq 0.15$.